



## Review

## Recent advances and key opportunities on in-plane micro-supercapacitors: From functional microdevices to smart integrated microsystems

Jieqiong Qin<sup>a,b,1</sup>, Hongtao Zhang<sup>b,1</sup>, Zhi Yang<sup>b</sup>, Xiao Wang<sup>a,c</sup>, Pratteek Das<sup>a,c</sup>, Feng Zhou<sup>a,c,\*</sup>, Zhong-Shuai Wu<sup>a,c,\*</sup>

<sup>a</sup>State Key Laboratory of Catalysis, Dalian Institute of Chemical Physics, Chinese Academy of Sciences, Dalian 116023, Liaoning, China

<sup>b</sup>College of Science, Henan Agricultural University, Zhengzhou 450002, Henan, China

<sup>c</sup>Dalian National Laboratory for Clean Energy, Chinese Academy of Sciences, Dalian 116023, Liaoning, China

## ARTICLE INFO

## Article history:

Received 19 December 2022

Revised 20 January 2023

Accepted 25 January 2023

Available online 16 February 2023

## Keywords:

Micro-supercapacitors

In-plane

Functionalization

Integrated microsystem

Energy storage

## ABSTRACT

The popularization of portable, implantable and wearable microelectronics has greatly stimulated the rapid development of high-power planar micro-supercapacitors (PMSCs). Particularly, the introduction of new functionalities (e.g., high voltage, flexibility, stretchability, self-healing, electrochromism and photo/thermal response) to PMSCs is essential for building multifunctional PMSCs and their smart self-powered integrated microsystems. In this review, we summarized the latest advances in PMSCs from various functional microdevices to their smart integrated microsystems. Primarily, the functionalities of PMSCs are characterized by three major factors to emphasize their electrochemical behavior and unique scope of application. These include but are not limited to high-voltage outputs (realized through asymmetric configuration, novel electrolyte and modular integration), mechanical resilience that includes various feats of flexibility or stretchability, and response to stimuli (self-healing, electrochromic, photo-responsive, or thermal-responsive properties). Furthermore, three representative integrated microsystems including energy harvester-PMSC, PMSC-energy consumption, and all-in-one self-powered microsystems are elaborately overviewed to understand the emerging intelligent interaction models. Finally, the key perspectives, challenges and opportunities of PMSCs for powering smart microelectronics are proposed in brief.

© 2023 Science Press and Dalian Institute of Chemical Physics, Chinese Academy of Sciences. Published by ELSEVIER B.V. and Science Press. All rights reserved.



**Jieqiong Qin** received her Ph.D. degree at Dalian Institute of Chemical Physics (DICP), Chinese Academy of Sciences (CAS), from 2016 to 2020, under the supervision of Prof. Zhong-Shuai Wu. Now she is a lecturer at College of Science, Henan Agricultural University. Her research focuses on the design and synthesis of 2D mesoporous materials for electrochemical energy storage devices, such as supercapacitors and batteries.



**Hongtao Zhang** is currently an M.S. candidate at Henan Agricultural University under the supervision of Dr. Jieqiong Qin. He received his B.S. from Henan Agricultural University in 2021. His current research is focused on the synthesis of 2D MXene-based composite materials for energy storage devices.

\* Corresponding authors.

E-mail addresses: [zhoufeng1107@dicp.ac.cn](mailto:zhoufeng1107@dicp.ac.cn) (F. Zhou), [wuzs@dicp.ac.cn](mailto:wuzs@dicp.ac.cn) (Z.-S. Wu).

<sup>1</sup> These authors contributed equally to this work.



**Zhi Yang** is pursuing an M.S. degree at Henan Agricultural University, under the supervision of Dr. Jieqiong Qin. He received the B.S. degree from Henan Agricultural University in 2019. His current research focuses on the controllable synthesis of 2D graphene-based mesoporous materials for micro-supercapacitors.



**Xiao Wang** obtained her Ph.D. degree from DICP, CAS under the supervision of Prof. Zhong-Shuai Wu. She currently works as a postdoctor at DICP, CAS, advised by Prof. Zhong-Shuai Wu and Chenglin Sun. Her research interests focus on graphene & 2D materials, flexible and planar electrochemical energy storage devices.



**Prateek Das** received his M.S. degree from the Indian Institute of Technology, Kharagpur in 2016 after which he joined Prof. Zhong-Shuai Wu's group at the DICP, CAS in 2017 as a Ph.D. candidate, under the sponsorship of CAS-TWAS President's Fellowship. His research interest involves the preparation of 2D materials and corresponding heterostructures for new-concept micro-supercapacitors.



**Feng Zhou** received his Ph.D. degree at the Lanzhou Institute of Chemical Physics, CAS in 2016, and worked as a postdoctoral fellow at DICP during 2016–2021. Then he became an associate Professor of 2D Materials Chemistry & Energy Applications at DICP, CAS. His research interests include the chemistry of graphene and ionic liquids, microscale electrochemical energy storage devices, and supercapacitors.



**Zhong-Shuai Wu** received his Ph.D. from the Institute for Metal Research, CAS in 2011, and worked as a postdoctoral fellow at the Max Planck Institute for Polymer Research in Mainz, Germany during 2011–2015. Then he became a full Professor and Group Leader of 2D Materials Chemistry & Energy Applications at DICP, CAS. In 2018, he was promoted to be a DICP Chair Professor. His research interests include the chemistry of graphene and 2D materials, surface and nanoelectrochemistry, microscale electrochemical energy storage devices, supercapacitors, batteries, and energy catalysis.

## 1. Introduction

The booming progress of portable, implantable, and wearable electronic devices, e.g., flexible microelectronics, intelligent nanor-

obots, wireless sensor networks, and personal health trackers has heightened the demand for miniaturized energy storage devices (MESDs) and their integrated microsystems [1–5]. Among various MESDs, micro-supercapacitors (MSCs) continue to attract intensive attention owing to their high power density, long cycle life, excellent flexibility, shape diversity, lightweight design, and minimal maintenance [6–10]. In our discussion, the MSCs generally refer to miniaturized supercapacitors with a total footprint area/volume of micron to centimeter-scale, which can be categorized as fiber-shaped [11,12], in-plane type (i.e., stacked and interdigital MSCs) [13,14] and three-dimensional (3D) type [15] according to device configurations. In particular, the planar MSCs (PMSCs) with interdigital architecture are superior in terms of compatibility and performance over the others, thanks to a separator-free structure, customizable patterning, reduced ion transport resistance, enhanced ion diffusion, sufficient contact between electrode materials and electrolyte, and feasible on-chip integration [14,16–18]. As a result, they can be easily integrated with other functional microdevices on one substrate to miniaturize the entire self-powered microsystems. Hence, PMSCs have been deemed as one of the most prevalent and hopeful candidates for MESDs in energy-related fields.

Based on the charge storage mechanism, the PMSCs are divided into electrochemical double-layer capacitors (EDLCs), pseudocapacitors (PCs), and hybrid capacitors (HCs) similar to traditional supercapacitors [19–21]. EDLCs store charges via the electrostatic adsorption/desorption of ions on the electrode-electrolyte interface, guaranteeing excellent charge/discharge rate, ultrahigh power density and superior cycling stability. Due to high electrical conductivity, large specific surface area (SSA), outstanding electrochemical stability and low cost, various carbon-based materials including activated carbon (AC), onion-like carbon, carbon nanotube (CNT) and graphene [22–27], have been known as representative electrode materials for EDLCs. By comparison, PCs store/release charges through fast and reversible redox reactions on or near the surface of electrodes or ion intercalation into the electrodes, yielding remarkably enhanced capacitance and energy density. Transition metal oxides [28–30] and conductive polymers (e.g., polypyrrole (PPy), polyaniline (PANI), and poly(3,4-ethylene dioxathiophene) (PEDOT)) [31,32] are typical electrode materials for PCs, but are often limited by unsatisfactory electrical conductivity and/or low cyclability. Besides, HCs composed of an EDLC-type electrode and a PC or battery-type electrode have been widely researched [17,33–35]. By coupling the advantages of EDLCs and PCs/metal-ion batteries, the HCs offer a wide voltage window, high energy and power densities, and outstanding cycling stability, which help fill the gap between supercapacitors and batteries. Currently, these three PMSCs with multiple innovative form factors are undergoing rapid progress for different application scenarios.

To assess the performance of PMSCs, areal/volumetric specific capacitance, energy density and power density are regarded as the key performance metrics [36,37]. Different from conventional supercapacitors, PMSCs are composed of electrode materials with negligible weight but have a well-defined size of the whole device. Therefore, areal and volumetric normalized performances based on the electrode (or device) footprints (i.e., areal/volumetric capacitance, energy density and power density) are more reasonable and significant than gravimetric values [20,25,38]. At present, most PMSCs adopt areal or/and volumetric parameters for the evaluation of their electrochemical performances. It is noted that PMSCs with microelectrodes of atomic thickness or thick electrode film consisting of complex pore structures generally employ areal metrics to evaluate their performance [15,39]. Furthermore, the working voltage, self-discharging, Coulombic efficiency, cycling stability and certain functionality are equally important in practical applications for various PMSCs.

Apart from energy storage, the PMSCs can be integrated with intriguing functionalities (e.g., high voltage, flexibility, stretchability, self-healing, electrochromism and photo/thermal response) to construct smart microdevices and self-power integrated microsystems for intelligent microelectronics [7,40,41]. To date, the advances of PMSCs have been summarized to a certain extent based on device configurations, electrode materials, electrolytes and microfabrication techniques [8,18,42–44]. However, a systematic summary of the latest development of PMSCs with diverse functions and on-chip integrated microsystems is absent. In this review, we summarize the up-to-date progress in functional PMSCs (including high-voltage, flexible/stretchable and stimuli-responsive devices) and corresponding smart integrated microsystems, i.e., energy harvester-PMSC integrated microsystem, PMSC-energy consumption integrated microsystem and all-in-one self-powered microsystem (Fig. 1). Furthermore, existing challenges and future perspectives of PMSCs are briefly highlighted.

## 2. High-voltage PMSCs

High-voltage power supply (e.g., PMSCs) is essential for the development of microelectronics and micromachines, such as intelligent robots, soft actuators, dielectric elastomers and sensor networks [45–47]. Therefore, the introduction of high-voltage feature into PMSCs can not only offer increased energy density for individual devices, but also extend their application domains. In the past few years, relentless efforts have been undertaken on three aspects of designing asymmetric electrode configuration

[17,48–50], developing high-voltage electrolyte [51–54], and constructing tandem integrated PMSCs [46,47,55,56] to achieve high-voltage output.

### 2.1. Asymmetric configuration

Designing asymmetric configuration with two different electrodes and/or dissimilar charge storage mechanisms represents an effective method to boost the operating voltage of PMSCs. By virtue of the complementary potential ranges of positive and negative electrodes, the constructed asymmetric MSCs (AMSCs) can realize maximum operating voltage of 4.0 V or more in the appropriate high-voltage electrolytes during charging-discharging processes. Compared with hybrid MSCs, AMSCs generally cover a wider range, including but not limited to EDLC//PC, PC//PC, and EDLC//battery (i.e., metal-ion hybrid MSCs) configurations [42,57].

EDLC//PC-type configuration generally employs one EDLC-type electrode as power source and one pseudocapacitive electrode as energy source, which guarantees expanded voltage window and consequently enhanced energy density. For example, Zheng et al. [48] developed a class of planar stacked AMSCs (EG//MP-PASCs) with capacitive electrochemically exfoliated graphene (EG) as negative electrode, pseudocapacitive  $\text{MnO}_2$ /PEDOT-poly(styrenesulfonate) (PH1000) as positive electrode, and BN nanosheets as separator (Fig. 2a). With polyvinyl alcohol (PVA)/LiCl gel electrolyte, the EG//MP-PASCs displayed a wide operating voltage of 1.8 V and outstanding volumetric energy density of  $8.6 \text{ mWh cm}^{-3}$  (Fig. 2b), outperforming their symmetric MSCs and some

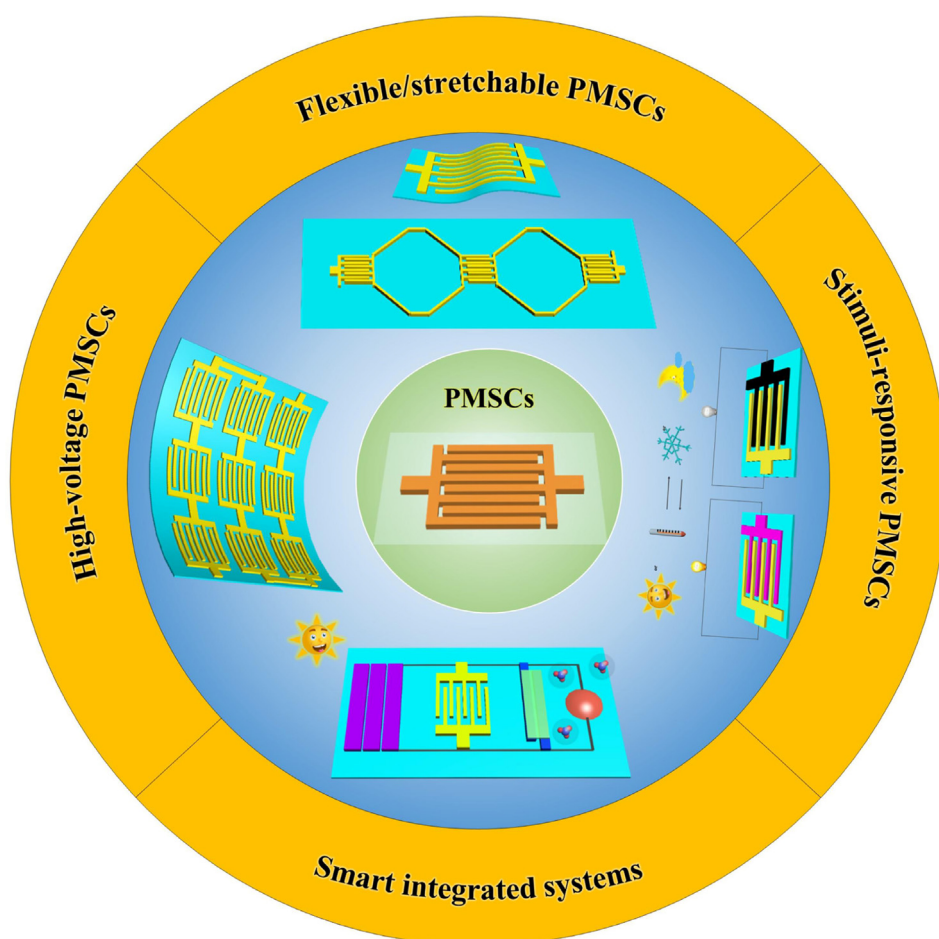
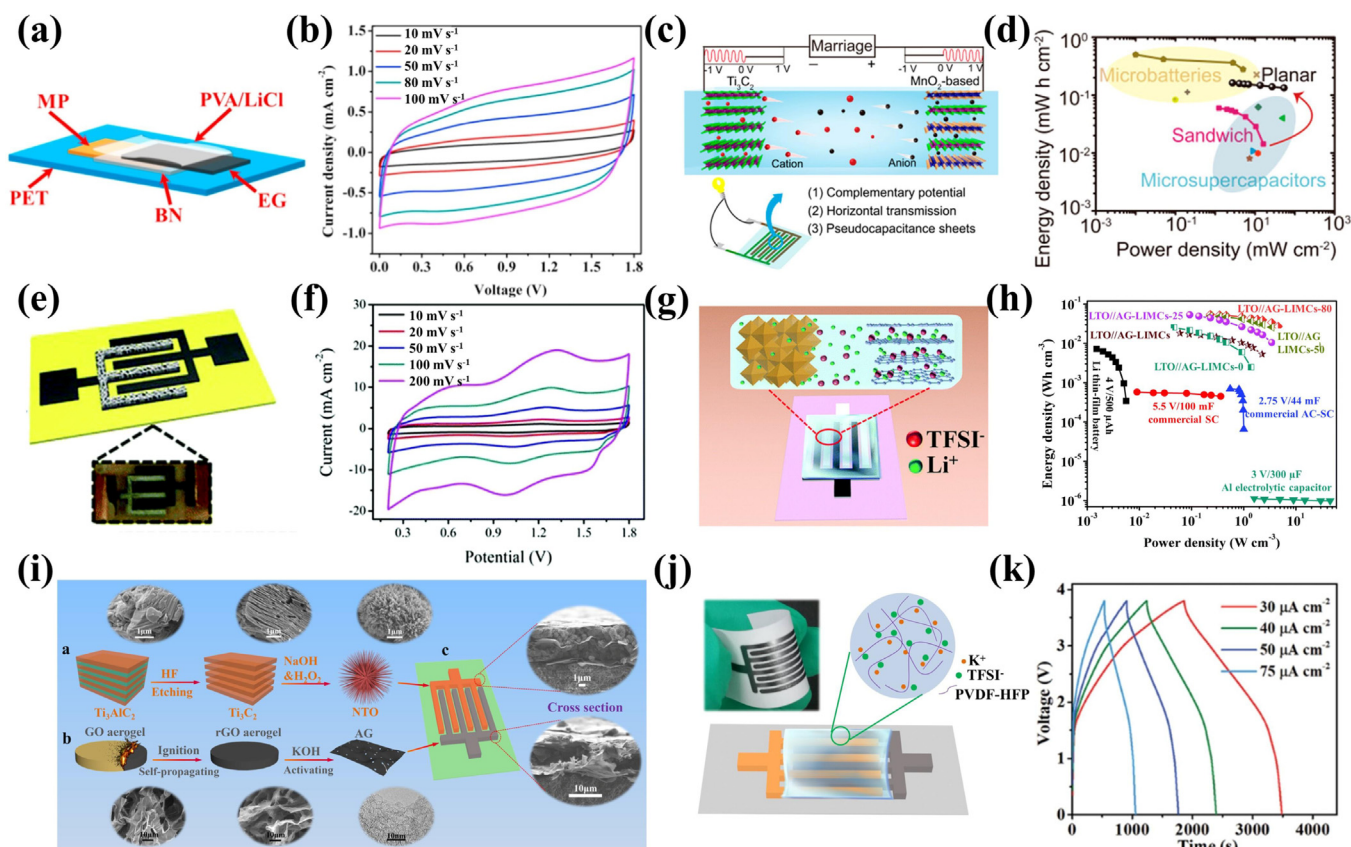


Fig. 1. Schematic illustration of PMSCs from functional microdevices to smart integrated microsystems.



**Fig. 2.** High-voltage PMSCs with asymmetric configuration. (a) Scheme of EG//MP-PASCs, and (b) CV curves of EG//MP-PASCs at varying scan rates. Reproduced with permission from Ref. [48], Copyright 2018, Elsevier. (c) Schematic illustration, and (d) Ragone plot of  $\text{Ti}_3\text{C}_2/\text{MnO}_2$  AMSC. Reproduced with permission from Ref. [69], Copyright 2020, American Chemical Society. (e) Schematic illustration, and (f) CV curves at varying scan rates for Zn-MSC. Reproduced with permission from Ref. [75], Copyright 2018, Royal Society of Chemistry. (g) Mechanism diagram of LTO//AG-LIMC, and (h) Ragone plot of LTO//AG-LIMC at diverse temperatures and other commercial energy storage devices. Reproduced with permission from Ref. [85], Copyright 2018, Royal Society of Chemistry. (i) Scheme of the assembly of Na-MSC with NTO anode and AG cathode. Reproduced with permission from Ref. [87], Copyright 2019, Wiley-VCH. (j) Schematic illustration and optical image, and (k) galvanostatic charge/discharge (GCD) profiles of K-MSC with KTO anode and AG cathode. Reproduced with permission from Ref. [88], Copyright 2021, Wiley-VCH.

reported AMSCs [58–60]. Moreover, EG//MP-PASCs exhibited admirable mechanical flexibility ( $\sim 98.8\%$  retention at a bending angle of  $180^\circ$ ), excellent adaptability to various substrates, and easy self-integration of three devices connected in series and parallel. More recently, a novel two-dimensional (2D) transition metal carbide/nitride, commonly known as MXene has emerged [61–64]. The metallic conductivity and high pseudocapacitance make it an ideal electrode candidate for high-performance PMSCs [38,65,66]. Considering the limited voltage window of  $\sim 0.6$  V for MXene-based symmetric MSCs, a planar interdigitated AMSC was fabricated comprising of  $\text{Ti}_3\text{C}_2\text{T}_x$  negative electrode, reduced graphene oxide (rGO) positive electrode and PVA/ $\text{H}_2\text{SO}_4$  gel electrolyte [67]. This  $\text{Ti}_3\text{C}_2\text{T}_x/\text{rGO}$  AMSC could operate reversibly at 1.0 V, and presented an energy density of  $8.6 \text{ mW h cm}^{-3}$  at power density of  $0.2 \text{ W cm}^{-3}$ . To further improve the voltage of MXene-based AMSCs, Yang's group employed  $\text{Ti}_3\text{C}_2\text{T}_x$ , AC and PVA/ $\text{Na}_2\text{SO}_4$  gel as negative electrode, positive electrode and electrolyte, respectively, to fabricate high-voltage AMSCs [68]. Notably, the  $\text{Ti}_3\text{C}_2\text{T}_x/\text{AC}$  AMSCs showed an enhanced voltage of 1.6 V, an energy density of  $3.5 \text{ mW h cm}^{-3}$  at  $100 \text{ mW cm}^{-3}$ , outstanding cycling stability of 91.4% retention for 10,000 cycles, and impressive integration ability in series or parallel. Additionally, the reduced energy density of  $\text{Ti}_3\text{C}_2\text{T}_x/\text{AC}$  AMSCs compared with  $\text{Ti}_3\text{C}_2\text{T}_x/\text{rGO}$  devices is derived from the different design of electrode materials, device geometry and electrolyte.

Another type of AMSCs is PC//PC configuration, which contains two different pseudocapacitive electrodes, e.g.,  $\text{Ti}_3\text{C}_2/\text{MnO}_2$  [69],  $\text{Ti}_3\text{C}_2\text{T}_x/\text{PPy}/\text{MnO}_2$  [70],  $\text{PPy}/\text{rGO}/\text{PEDOT}/\text{rGO}$  [71], graphene-VN

quantum dots (G-VNQDs)/rGO/V $_2\text{O}_5$ /rGO [72], and VN/ $\text{MnO}_2$  AMSCs [49]. This configuration is generally adopted to enhance the voltage window by pairing pseudocapacitive materials with suitable working potentials and boosting the overall electrochemical performance. For instance, Geng and coworkers demonstrated a  $\text{Ti}_3\text{C}_2/\text{MnO}_2$  AMSC by combining pseudocapacitive  $\text{Ti}_3\text{C}_2$  and  $\text{MnO}_2$  nanosheets with complementary working potentials of  $-0.95-0$  V and  $0-1.0$  V vs. Ag/AgCl, respectively (Fig. 2c) [69]. The device exhibited a large voltage window of 2.0 V, excellent rate performance with 83% retention at a 20-fold current density, high energy density of  $162 \mu\text{W h cm}^{-2}$ , and maximum power density of  $54 \text{ mW cm}^{-2}$  (Fig. 2d). In another work, 2.4 V aqueous AMSCs were assembled by VN nanosheet arrays as negative electrode and Na- $\text{MnO}_x$  nanosheets on 3D nitrogen-doped carbon fiber (Na- $\text{MnO}_x$ @NCF) as positive electrode in carboxymethyl cellulose sodium (CMC)/ $\text{Na}_2\text{SO}_4$  gel electrolyte [73]. The large voltage window and excellent pseudocapacitive behavior endowed this AMSCs with exceptional areal capacitance ( $109.5 \text{ mF cm}^{-2}$ ) and energy density ( $87.62 \mu\text{W h cm}^{-2}$ ). These studies provided effective approach for exploiting high-voltage aqueous AMSCs by choosing wide-voltage positive and negative electrodes and using stable neutral electrolytes.

Metal-ion hybrid MSCs are composed of an EDLC-type and a battery-type electrodes, integrating high power density and long cycle life of EDLCs with high energy density of batteries in a single device [35,74]. In recent years, the prevalent metal-ion hybrid MSCs contain aqueous Zn-ion MSCs (Zn-MSCs) [75–83] and Mg-ion MSCs (Mg-MSCs) [84], organic Li-ion MSCs (Li-MSCs) [52,85], Na-ion MSCs (Na-MSCs) [86,87] and K-ion MSCs (K-MSCs) [88].

For example, Qu and coworkers developed an interdigital Zn-MSC with metal zinc anode and capacitive CNT cathode by laser carving and subsequent electroplating processes (Fig. 2e) [75]. With gelatin/ZnSO<sub>4</sub> gel electrolyte, the Zn-MSC revealed a voltage range of 0.2–1.8 V (Fig. 2f), impressive areal capacitance of 83.2 mF cm<sup>-2</sup>, and 87.4% capacitance retention for 6000 cycles. Significantly, the maximum areal energy and power densities are 29.6 μW h cm<sup>-2</sup> and 8 mW cm<sup>-2</sup>, respectively, higher than those of other reported aqueous PMSCs [89–91]. Inspired by this, various Zn-MSCs including Zn//poly(3,3'-dihydroxybenzidine)/AC [76], Zn//AC [77], Zn//phosphorene [78], Zn//biomass kelp-carbon [79], Zn//porous carbon framework (PCF) [81], and Zn//Ti<sub>3</sub>C<sub>2</sub>T<sub>x</sub> cells [82] have also been demonstrated. Their operating voltage was boosted to 2.2 V [78], and the maximum areal energy density was ~152 μW h cm<sup>-2</sup> [76], offering novel insights into designing high-voltage and long-life MESDs with desirable safety. Such hybrid devices can also be printed, as demonstrated by inkjet-printing planar Mg-MSCs with 3D crumpled MoS<sub>2</sub> as negative and rGO as positive electrodes [84]. The Mg-MSCs delivered a stable operating voltage (1.75 V), superior cycling stability (96% retention after 20,000 cycles), and outstanding areal energy density (3.85 μW h cm<sup>-2</sup>) and power density (12.6 mW cm<sup>-2</sup>) in 1 M MgSO<sub>4</sub> electrolyte. Meanwhile, nonaqueous Li-MSCs [52,85], Na-MSCs [86,87] and K-MSCs [88] are undergoing unprecedented development. As shown in Fig. 2 (g), our group demonstrated a novel prototype of Li-MSCs (LTO//AG-LIMCs) based on lithium titanate (LTO) nanospheres as anode and activated graphene (AG) as cathode with ionogel electrolyte (LiTFSI-P<sub>14</sub>TFSI-PVDF-HFP) containing bis(trifluoromethanesulfonyl)imide lithium salt (LiTFSI), 1-butyl-1-methylpyrrolidinium bis(trifluoromethyl-sulfonyl)imide (P<sub>14</sub>TFSI) and poly(vinylidene difluoride-co-hexafluoropropylene) (PVDF-HFP) [85]. The as-fabricated Li-MSCs exhibited high working voltage of 3.0 V, and admirable volumetric energy density of 53.5 mW h cm<sup>-3</sup>, exceeding most of the previously reported MSCs (Fig. 2h) [92,93]. Owing to the advanced device configuration and highly stable ionogel electrolyte, their mechanical flexibility, series/parallel integration, thermal stability and safety were also prominent. Further, the increasing price and low natural abundance of lithium have triggered researchers to develop alternatives of high-voltage Na-MSCs and K-MSCs. Recently, our group also explored advanced Na-MSCs with urchinlike sodium titanate (NTO) anode and AG cathode [87], and K-MSCs based on MXene-derived potassium titanate (KTO) anode and AG cathode (Fig. 2i–k) [88]. With non-flammable ionogel electrolyte of bis(trifluoromethanesulfonyl)imide sodium salt (NaTFSI)-P<sub>14</sub>TFSI-PVDFHFP and bis(trifluoromethylsulfonyl)imide potassium salt (KTFSI)-P<sub>14</sub>TFSI-PVDFHFP, the resulting Na-MSCs and K-MSCs revealed wide operating voltages of 3.5 and 3.8 V, as well as extraordinary energy densities of 37.1 and 34.1 mW h cm<sup>-3</sup>, respectively. Moreover, both of them displayed good cycling stability, robust mechanical flexibility and facile integration. Clearly, these planar metal-ion hybrid MSCs with large voltage and high energy density offer great prospects for designing high-performance MESDs for microelectronics.

Lastly, AMSCs with one pseudocapacitive and one battery-type electrodes have also been reported but currently show subpar overall performance. For example, aqueous VN//Co(OH)<sub>2</sub> MSCs [50], Ti<sub>3</sub>C<sub>2</sub>T<sub>x</sub>//V<sub>2</sub>O<sub>5</sub> Zn-MSCs [83] and PPy@FeOOH//Mn<sub>3</sub>O<sub>4</sub> Mg-MSCs [94] can achieve high energy density, but the relatively sluggish dynamics and inferior cycle life still need further improvement for applications in the future.

## 2.2. High-voltage electrolytes

Apart from the asymmetric device configuration, the electrolyte is considered another crucial factor to determine the working voltage of PMSCs [8,51,95–97]. At present, the commonly used elec-

trolytes are classified into three types of aqueous electrolyte (ions in water) [98–100], organic electrolyte (salts in organic solvents) [95,101] and ionic liquid (IL, pure molten salts) [102,103]. To prevent the leakage risk, quasi/all-solid-state electrolytes have been produced by adding soluble polymers (e.g., PVA, poly(ethylene) oxide (PEO) and poly(acrylate)) or inorganic fillers (e.g., nano-silica) into these liquid electrolytes [49,104–107].

Firstly, the aqueous electrolytes of acids, alkalis and salts have been widely used in PMSCs owing to their small ion sizes, large ionic conductivity, low price, and eco-friendliness [98–100]. Unfortunately, the operating voltage of symmetric PMSCs with aqueous electrolytes is limited to 1.23 V, deriving from the low decomposition potential of H<sub>2</sub>O. Since “water-in-salt” (WIS) electrolyte of 21 m (mol kg<sup>-1</sup>) LiTFSI was reported for high-voltage aqueous Li-ion battery achieving 2.3 V in 2015 [108], various highly concentrated WIS electrolytes have been applied in MESDs [99,109–111]. For example, our group demonstrated a low-cost, highly safe WIS electrolyte of 20 m LiCl to broaden the voltage window of MXene-based PMSCs (MXene-MSCs) [53]. As exhibited in Fig. 3(a and b), the molecular dynamics simulations revealed that most H<sub>2</sub>O molecules are strongly coordinated with Li<sup>+</sup> ions in 20 m LiCl, thus offering reduced activity of H<sub>2</sub>O molecules and improved electrochemical stability of WIS electrolyte. Further, the WIS gel electrolyte of SiO<sub>2</sub>/LiCl ensured the symmetric MXene-MSCs with high operating voltage of 1.6 V (Fig. 3c), outstanding volumetric energy density of 31.7 mW h cm<sup>-3</sup>, and impressive environmental adaptability between –40 to 60 °C. Meanwhile, Liu et al. [89] reported an all-3D-printed PMSCs consisting of AC-based ink electrode and WIS gel electrolyte prepared from SiO<sub>2</sub>/LiCl (Fig. 3d). Thanks to the stable voltage window of WIS electrolyte (20 m LiCl) and the high electrochemical stability of AC-based electrode, the as-fabricated PMSCs realized steady operation at a high voltage of 2.0 V and presented high areal energy density of 331 μW h cm<sup>-2</sup>, far beyond those of other aqueous symmetric MSCs [71,112]. Recently, this WIS gel electrolyte of SiO<sub>2</sub>/LiCl was also applied in aqueous MXene//MnO<sub>2</sub> AMSCs, which submitted a ultrahigh voltage of 2.4 V and an exceptional volumetric energy density of 53 mW h cm<sup>-3</sup> [113]. On the whole, the aqueous WIS electrolytes have opened a new horizon for designing high-voltage and safe PMSCs.

Secondly, replacing aqueous electrolytes with organic electrolytes can effectively enlarge the operating voltage of PMSCs, attributing to the high decomposition voltages of organic solvents, e.g., ethylene carbonate (EC), propylene carbonate (PC), dimethyl carbonate (DMC) and acetonitrile [42,52,86]. However, the relatively large ion size, high viscosity, toxic nature and flammability make organic electrolytes rarely applicable in PMSCs. So far, the representative Li-MSC and Na-MSC with traditional organic electrolytes have been reported [52,86]. With AC positive electrode, pre-lithiated graphite negative electrode and 1 M LiPF<sub>6</sub> (in EC/DMC) electrolyte, as-fabricated Li-MSC exhibited a wide working voltage of 0.1–3.8 V, and superior areal energy density of 486 μW h cm<sup>-2</sup> [52]. Meanwhile, Na-MSC based on VS<sub>2</sub>@EG anode and AC cathode delivered a working voltage of 0.01–3.5 V in 1 M NaClO<sub>4</sub> organic electrolyte, and thus provided an areal energy density of 188.3 μW h cm<sup>-2</sup> at 0.35 mW cm<sup>-2</sup> [86]. Given the strengths and weaknesses of aqueous and organic electrolytes, combining WIS and organic solvent may produce a novel electrolyte with relatively high voltage, decreased viscosity, enhanced ionic conductivity, and improved safety [114,115]. Using this concept, Jin et al. [115] demonstrated a polyacrylamide polyelectrolyte (HVTT-PAM) by soaking porous polyacrylamide gel in 10.5 m LiTFSI water/ethylene glycol solution, achieving a landmark voltage of 2.3 V for CNT-based symmetric PMSCs (Fig. 3e). Also, the as-fabricated PMSCs revealed high areal energy density (≥4.9 μW h cm<sup>-2</sup>) and remarkable cycling stability at temperatures

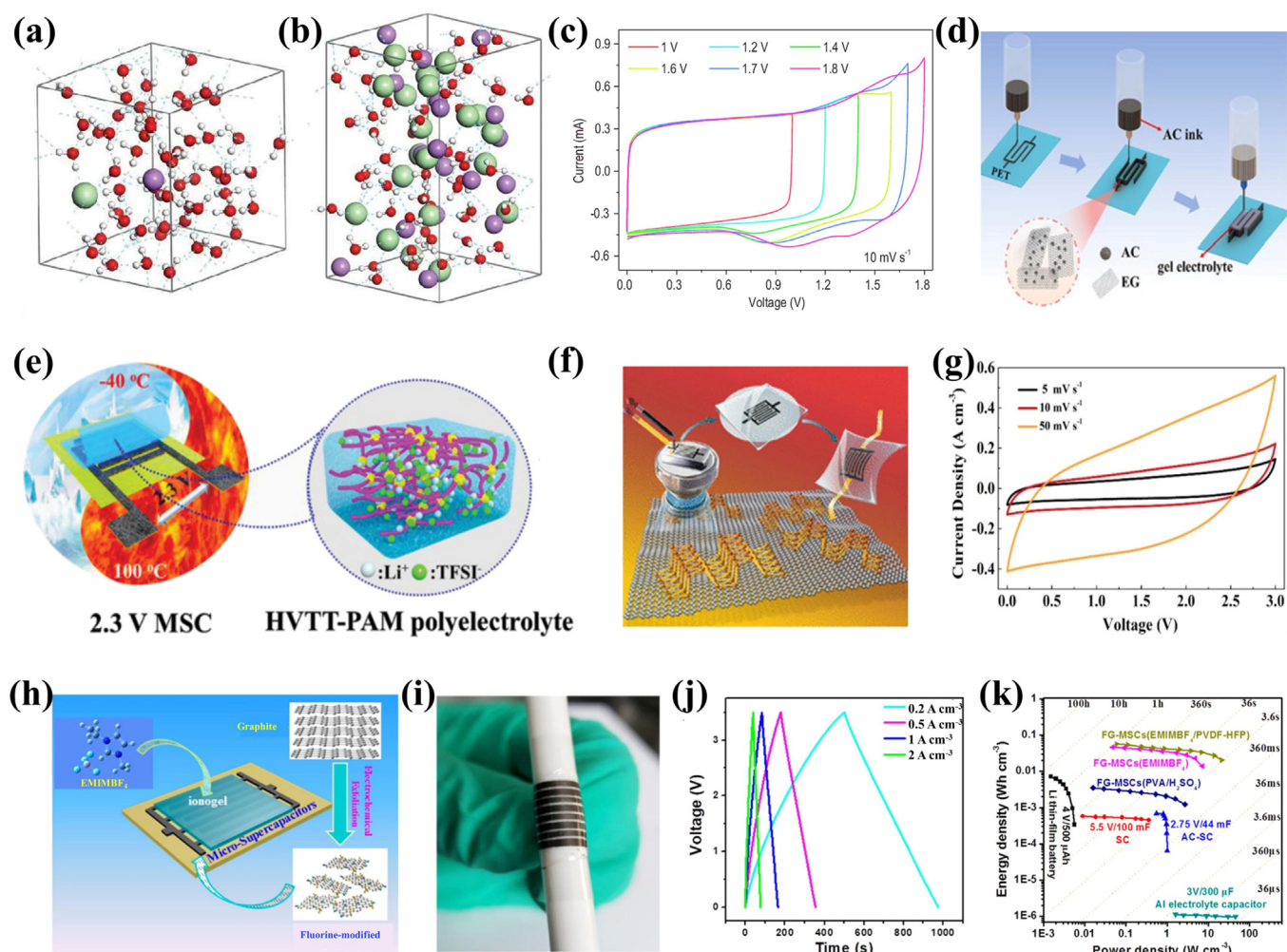


**Fig. 3.** High-voltage PMSCs with high-voltage electrolytes. (a, b) Molecular dynamics simulation diagrams of (a) 1 m LiCl and (b) 20 m LiCl electrolytes (Atom colors: Li-purple; Cl-green; O-red; H-white), and (c) CV curves of MXene-MSC with varying voltage windows. Reproduced with permission from Ref. [53], Copyright 2022, Oxford University Press. (d) Scheme of the fabrication of all-3D-printed PMSCs with WIS gel electrolyte. Reproduced with permission from Ref. [89], Copyright 2021, Elsevier. (e) Schematic illustration of HVTT-PAM polyelectrolyte and corresponding high-voltage PMSC. Reproduced with permission from Ref. [115], Copyright 2021, Wiley-VCH. (f) Scheme of the fabrication, and (g) CV curves of PG-MSC. Reproduced with permission from Ref. [117], Copyright 2017, American Chemical Society. (h) Scheme of the fabrication, (i) photograph at a bending state, (j) GCD profiles, and (k) Ragone plot of FG-MSCs. Reproduced with permission from Ref. [54], Copyright 2018, American Chemical Society.

from  $-40$  to  $100$  °C, confirming the superiority and applicability of HVTT-PAM. Moreover, Wu and coworkers developed a hybrid gel electrolyte (HGE) with 10 m LiCl in  $\text{H}_2\text{O}$ /ethylene glycol mixed solvents for high-performance PMSCs [116]. It is worth noting that ethylene glycol could effectively break hydrogen bond networks between  $\text{H}_2\text{O}$  molecules, providing a high electrochemical stability window of 2.7 V and low glass-transition temperature of  $-62.8$  °C. Using this HGE, the symmetric PMSCs based on AC active materials exhibited stable operating voltage (1.6 V), high energy density ( $10.3 \text{ mW h cm}^{-3}$ ), long cyclability (85.7% retention for 15,000 cycles), and impressive low-temperature performance (68.3% retention at  $-30$  °C). Therefore, the hybrid organic/WIS electrolyte may offer a novel avenue for high-voltage, high-energy and anti-freezing MESDs.

Thirdly, room-temperature IL electrolytes have also been extensively applied in PMSCs due to their wide operating window of  $>4.0$  V, low vapor pressure, good thermal stability, and non-flammability [102,103]. As displayed in Fig. 3(f), our group developed the mask-assisted fabrication of high-energy-density PMSCs (PG-MSCs) with hybrid microelectrodes of phosphorene and EG

nanosheets in IL electrolyte of 1-butyl-3-methylimidazolium hexafluorophosphate (BMIMPF<sub>6</sub>) [117]. By virtue of the elaborated design and selection of 2D active materials, device microfabrication and IL electrolyte, the PG-MSCs delivered outstanding electrochemical performance, such as wide working voltage of 3.0 V (Fig. 3g), high energy density of  $\sim 11.6 \text{ mW h cm}^{-3}$ , good flexibility and superior integration. Furthermore, Zhou et al. [54] demonstrated high-quality fluorine-modified graphene (FG) for high-performance ionogel-based MSCs (FG-MSCs) through one-step electrochemical exfoliation of graphite (Fig. 3h and i). With the IL ionogel electrolyte of 1-ethyl-3-methylimidazolium tetrafluoroborate (EMIMBF<sub>4</sub>)-PVDF-HFP, the FG-MSCs revealed large voltage window of 0–3.5 V (Fig. 3j), admirable volumetric energy density of  $56 \text{ mW h cm}^{-3}$  (Fig. 3k), excellent flexibility with  $\sim 100\%$  capacitance retention at  $180^\circ$ , and efficient integration in series/parallel. Although the IL electrolyte has been regarded as a promising candidate for realizing high-safety, high-voltage and high-energy PMSCs, its strong viscosity, low ionic conductivity and high sensitivity to moisture should be taken into account during practical applications.

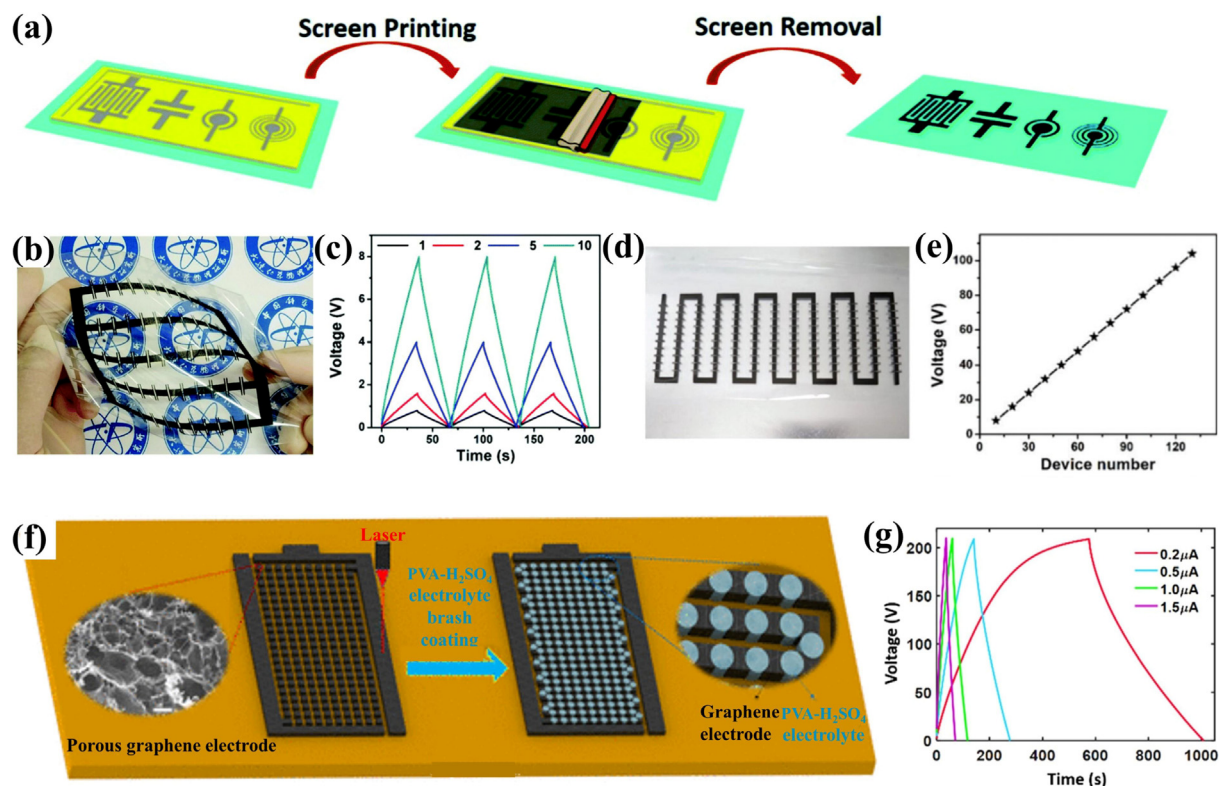


**Fig. 4.** High-voltage PMSCs with modular integration. (a) Scheme of the universal fabrication process, (b) photograph in twisted state, (c) GCD profiles with serial fashion, (d) photograph of a tandem pack of 130 cells, and (e) output voltage with cell number for SPG-IMSCs. Reproduced with permission from Ref. [46], Copyright 2019, Royal Society of Chemistry. (f) Schematic illustration of the construction, and (g) GCD profiles at different currents for integrated PMSC pack with 209 tandem units based on laser-induced graphene. Reproduced with permission from Ref. [55], Copyright 2018, American Chemical Society.

### 2.3. Modular integration of PMSCs

For a single PMSC with asymmetric configuration and high-voltage electrolyte, the intrinsic working voltage is normally limited to 4.0 V [25,42]. Considering the planar geometry advantage of PMSCs built on one substrate, constructing compact integrated MSC pack will be a feasible and efficient strategy to realize ultrahigh-voltage output. Along these lines, Shi et al. [46] developed high-voltage integrated PMSCs (SPG-IMSCs) based on screen-printed graphene (SPG) ink, as illustrated in Fig. 4(a). Specifically, the SPG-IMSCs with different planar geometries could be screen-printed in several seconds, possessing metal-free interconnects, superior flexibility, and tailored capacitance and voltage (Fig. 4b and c). As demonstrated, tandem SPG-IMSCs with 130 cells delivered an ultrahigh voltage of >100 V, indicating the impressive modularization and uniformity of SPG-IMSCs (Fig. 4d and e). In another work, 210 of square microelectrodes were fabricated by a direct laser-writing on polyimide film, generating integrated PMSCs connected in series of 209 units with a recorded voltage output of 209 V (Fig. 4f and g) [55]. By adjusting microelectrode array and output voltage, the integrated MSC pack could effectively power a piezoresistive microsensors needing 6 V and a walking microrobot requiring >2000 V for activation. Overall, these studies pave a reliable way for scalable fabrication of planar integrated MEDSs to power well-defined high-voltage microelectronics.

Obviously, these three strategies, i.e., innovative asymmetric electrode configuration (EDLC//PC, PC//PC, and EDLC//battery), high-voltage electrolyte (concentrated WIS, hybrid organic/WIS and IL), and tandem integrated pack do realize enhanced voltage considering electrode, electrolyte and integration, respectively. The next step would be a reasonable combination of these three strategies, which may be a challenging yet promising direction to

improve the total output voltage up to several kV. In the near future, these high-voltage and high-energy PMSCs can effectively meet the practical commercial applications for high-voltage microelectronics and micromachines.

## 3. Flexible and stretchable PMSCs

To satisfy the demands of wearable and implantable applications, flexibility and stretchability are important attributes that PMSCs should acquire to withstand the deformation against external strain, such as muscle motions and joint movement [7,41,118]. In principle, through rational designs of electrode materials and structures, the mechanical tolerance of PMSCs can be improved to achieve flexibility and stretchability for on-chip microelectronics. Therefore, considerable efforts have been focused on developing high-performance flexible and stretchable PMSCs with arbitrary shape in recent years.

### 3.1. Flexible PMSCs

The material selection, structure design and microfabrication strategies play key roles in implementing the flexibility of PMSCs [118–120]. From the material point of view, the electrodes, electrolytes, substrates and current collectors should retain their original functions under different deformation states and repetitive mechanical distortions. Further, the electrode/device structure and assembly technology are determined by the target requirements and specific application scenarios of flexible PMSCs.

Benefiting from the planar thin-film electrodes, quasi-solid-state gel electrolytes, and diverse flexible substrates, a large number of flexible PMSCs with designable structure have been

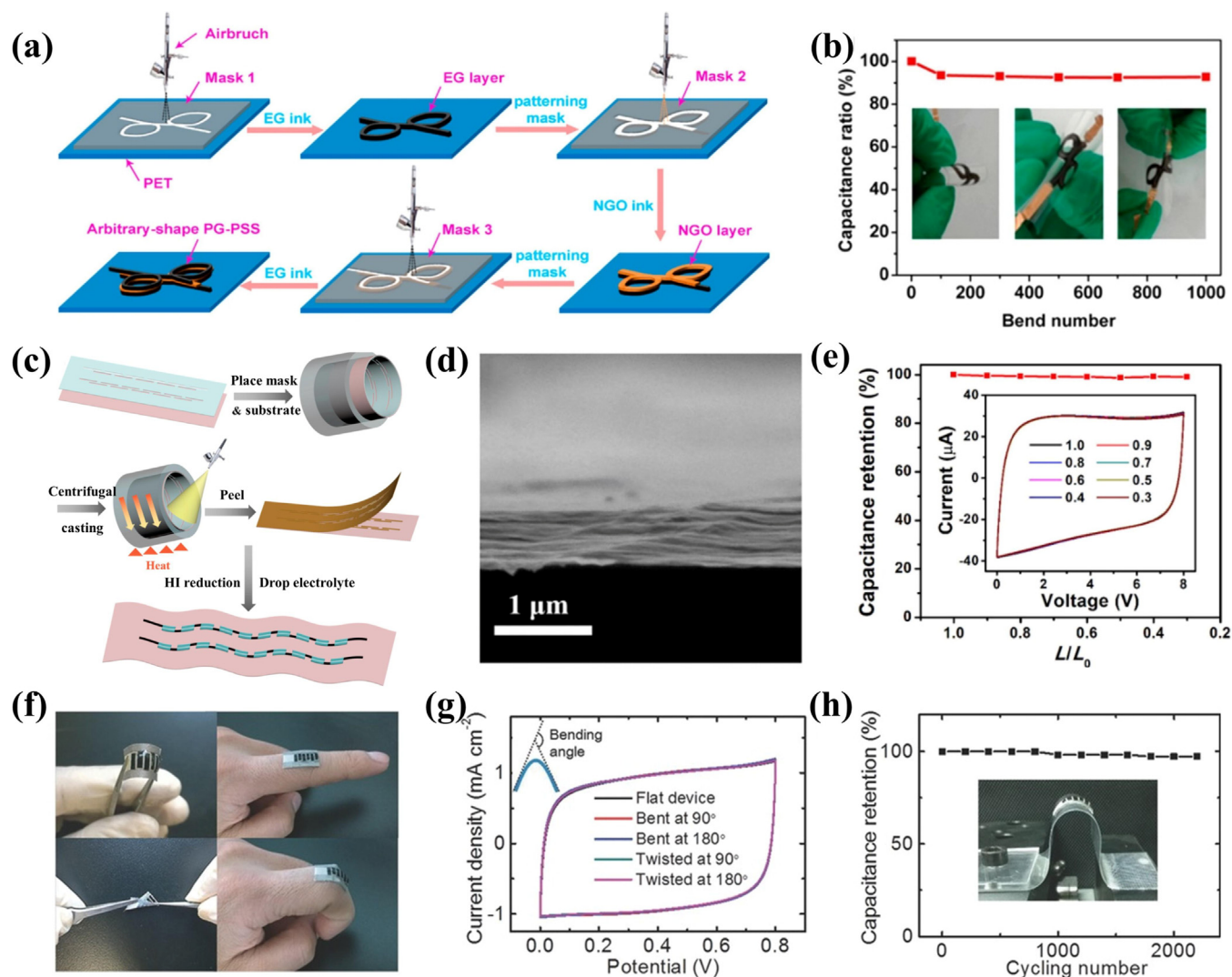


**Fig. 5.** Flexible PMSCs. (a) Schematic illustration of the fabrication process, and (b) capacitance retention versus bending cycles for junction-wire-shaped PG-PSSs. Reproduced with permission from Ref. [126], Copyright 2017, American Chemical Society. (c) Scheme of the fabrication of flexible PMSCs by MCCC technique, (d) cross-section SEM image of rGO-PH1000 electrode film, and (e) mechanical flexibility of MCCC-MSCs at varying bending states (Inset: CV curves at  $500 \text{ mV s}^{-1}$ ). Reproduced with permission from Ref. [127], Copyright 2021, Elsevier. (f) Optical images under diverse bending/twisting states, (g) CV curves at varying bending/twisting angles, and (h) capacitance retention versus bending numbers for textile PMSCs. Reproduced with permission from Ref. [128], Copyright 2016, Wiley-VCH.

developed using various microfabrication methods [121–128]. For example, flexible sandwich-like PMSCs (denoted as PG-PSSs) were developed on one substrate by spray printing, in which both the electrodes were comprised of 2D EG and electrically insulating 2D GO (100 nm in lateral size) served as a separator (Fig. 5a) [126]. Remarkably, the PG-PSSs presented excellent mechanical flexibility of >93.0% capacitance retention under continuous bending cycles for 1000 times (Fig. 5b). Also, they could realize various customized shapes including rectangle, hollow-square, circle, junction-wire and “A”, “1” and “2” characters, outstanding volumetric capacitance of  $\sim 280 \text{ F cm}^{-3}$ , long cycle life of 93% retention for 10,000 cycles, and facile integration in series or parallel. This work confirmed the advantages of all-2D-material design and printing technique for constructing flexible and high-performance PMSCs.

Furthermore, linear PMSCs have garnered considerable attention owing to easy processing, accessible integration and excellent flexibility. For instance, our group reported a mask-assisted continuous centrifugal coating (MCCC) technique to fabricate flexible and linear tandem PMSCs with rGO-PH1000 hybrid electrode films

(Fig. 5c) [127]. The simple and scalable MCCC strategy provided strong centrifugal and shear forces for assembling flexible rGO-PH1000 electrode films with high compactness and packing density (Fig. 5d). Using PVA/ $\text{H}_2\text{SO}_4$  gel electrolyte and soft polyethylene terephthalate (PET) substrate, as-fabricated MCCC-MSCs displayed superior mechanical flexibility under different bending states (Fig. 5e), impressive volumetric energy density of  $\sim 2.8 \text{ mW h cm}^{-3}$ , and good integration. The outstanding electrochemical performance and flexibility were derived from the effective coupling of high-density active material film and advanced MCCC fabrication.

In addition, a new-concept interdigital, textile PMSCs were demonstrated through mask-assisted Ni-deposition and rGO-coating on different textile substrates [128]. With PVA/ $\text{H}_3\text{PO}_4$  gel electrolyte, the textile PMSCs achieved an areal capacitance of  $8.19 \text{ mF cm}^{-2}$ , impressive cycling performance of 91% for 10,000 cycles, and exceptional rate capability of 53% retention from 0.01 to  $2 \text{ V s}^{-1}$ . More importantly, the textile PMSCs revealed superior mechanical flexibility and electrochemical stability, i.e., no noticeable degradation of CV curves under severe bending and twisting

conditions, and 97.2% capacitance retention after 2000 bending cycles (Fig. 5f–h). Hence, the textile PMSCs provide a new possibility for powering flexible and wearable electronics.

It is well known that most PMSCs possess good flexibility at various bending states due to the structural superiority of thin-film microelectrodes, soft 2D substrate and planar device configuration. For truly flexible PMSCs, the cycling stability under repetitive bending or twisting is the primary metric. Therefore, the full combination of flexible material and device structure, and applicable microfabrication technologies is of significant importance to realize absolutely flexible PMSCs for wearable and implantable applications.

### 3.2. Stretchable PMSCs

By implementing a stretchability of 30% strain, the PMSCs can well accommodate human motions for wearable electronic skins, electronic textiles and health monitors [129,130]. In the recent years, three main strategies have been proposed to develop stretchable PMSCs and PMSC-arrays by elaborately selecting flexible materials [112,131–134], engineering stretchable microelec-

trodes [135–138], and designing stretchable array structure [139–143].

The first point of focus is the flexibility of individual components which include active materials of electrode, mechanically reinforced electrolyte, elastic substrate and encapsulation, which are indispensable during the fabrication of stretchable PMSCs. As a prime example, intrinsically stretchable PMSCs with ordered honeycomb-like porous interdigitated microelectrodes were demonstrated by a 3D printing technique [112]. To be specific, a pseudoplastic gel-like ink composed of MXene nanosheets, manganese dioxide nanowires (MnONWs), silver nanowires (AgNWs) and fullerene (C60) was prepared, and subsequently deposited onto polydimethylsiloxane (PDMS) substrate by an extrusion-based 3D printing technique. After unidirectional freezing, a honeycomb-like hierarchical porous structure with oriented lamella cell walls was generated (Fig. 6a–c). With PVA/KOH gel electrolyte, the resulting PMSCs revealed high electrochemical performance including energy density of  $19.2 \mu\text{Wh cm}^{-2}$ , power density of  $58.3 \text{ mW cm}^{-2}$ , and mechanical stretchability with <20% degradation under 50% tensile strain and  $\sim 75\%$  retention after 1000 stretching/releasing cycles (Fig. 6d). The excellent performance could be attributed to the coupling effects of high-active

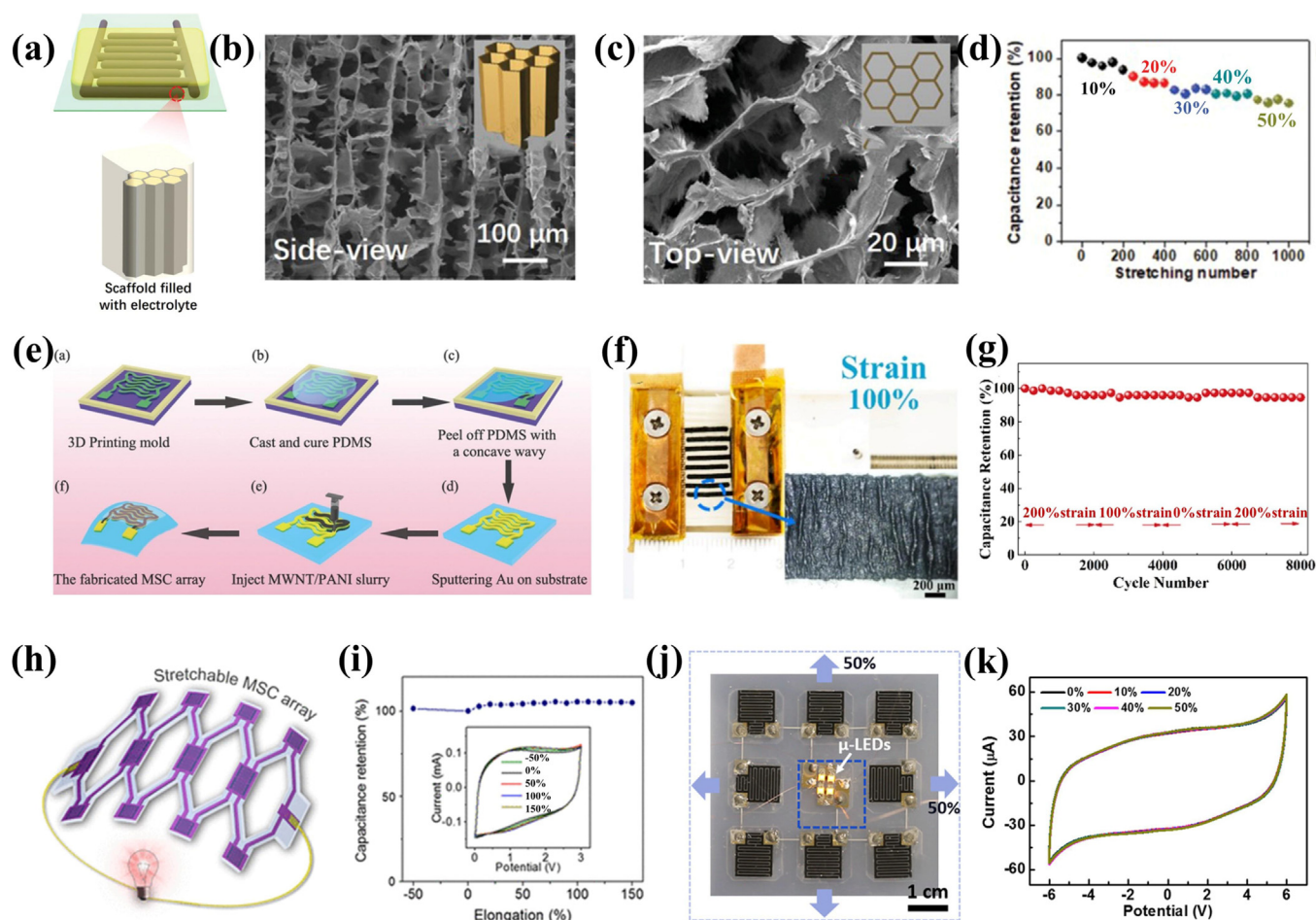


**Fig. 6.** Stretchable PMSCs and PMSC-arrays. (a) Scheme of the stretchable PMSCs with honeycomb-like porous electrode, (b) cross-section SEM image, and (c) top-view SEM image of honeycomb-like porous electrode, (d) capacitance retention with stretching/releasing cycles for the stretchable PMSCs under different strains. Reproduced with permission from Ref. [112], Copyright 2020, Wiley-VCH. (e) Scheme of the fabrication process of wave-shaped stretchable PMSCs. Reproduced with permission from Ref. [135], Copyright 2017, Wiley-VCH. (f) Photograph of device and SEM image of microelectrode of GCP-MSCs at a strain rate of 100%, and (g) cycling stability of GCP-MSCs under different strain states. Reproduced with permission from Ref. [136], Copyright 2018, Elsevier. (h) Schematic diagram, and (i) cycling stability versus elongation for stretchable PMSC-arrays with honeycomb-like substrate and interconnection. Reproduced with permission from Ref. [139], Copyright 2016, American Chemical Society. (j) Optical image under biaxial strain of 0%, and (k) CV curves as a function of biaxial strains for the biaxially stretchable PMSC-arrays. Reproduced with permission from Ref. [140], Copyright 2014, American Chemical Society.

MXene and MnONWs, high-conductive AgNW networks, slideable C60 nanoparticles and stretchable honeycomb-like porous electrode structure.

Second, constructing stretchable microelectrode is also crucial to readily achieve stretchable PMSCs. Generally, the geometrical structures of microelectrodes for this purpose are wavy, wrinkly and reticulated, which allow the electrode and device to flatten out to release strain under stretching. For instance, Li et al. [135] developed highly stretchable PMSCs with wave-shaped hybrid multiwalled CNT (MWCNT)/PANi electrodes by 3D printing strategy (Fig. 6e). Owing to the unique design of concave wave electrode structure and the usage of stretchable PDMS substrate, the resulting PMSCs revealed good electrochemical stability under varying stretching states (up to 40%). Moreover, the stretchable MSCs presented high areal capacitance ( $44.13 \text{ mF cm}^{-2}$ ), impressive energy density ( $0.004 \text{ mW h cm}^{-2}$ ) and power density ( $0.07 \text{ mW cm}^{-2}$ ), originating from the good conductivity of MWCNTs and high pseudocapacitance of PANi nanorods. Besides, our group demonstrated highly stretchable PMSCs (GCP-MSCs) with wrinkled interdigital electrode patterns of EG/CNT/PH1000 film (GCP) on an elastic rubber substrate (Fig. 6f) [136]. In stretchable GCP, the cross-linked PH1000 and wrapped CNTs served as a stretchable skeleton and capacitance supplier, and 2D EG acted as conductivity enhancer, endowing rapid ion–electron transport and robust interface interaction. After coating with gel electrolyte of PVA/H<sub>3</sub>PO<sub>4</sub>, the GCP-MSCs displayed excellent stretchability up to 200%, and admirable cyclability under repeated tensile states (93.2% capacitance retention over 8000 cycles, Fig. 6g). Therefore, the elaborate design of stretchable microelectrodes can endow stretchable PMSCs with both high electrochemical performance and superior stretchability.

Third, designing stretchable arrays including the usage of stretchable interconnects and/or deformable substrates is regarded as an effective strategy to achieve stretchable PMSC pack for wearable electronics. As an example, highly stretchable PMSC-arrays on honeycomb-like PDMS substrates were demonstrated using single-walled CNT (SWCNT) microelectrode and PVA/H<sub>3</sub>PO<sub>4</sub> gel electrolyte (Fig. 6h) [139]. The unique honeycomb structure of interconnects and substrates endowed PMSC-arrays with negligible strain during stretching and facile integration with other electronics. As a result, the PMSC-arrays displayed excellent mechanical stability under 150% stretching, 180° bending, and 60° twisting (Fig. 6i). Moreover, introducing the stiff islands to soft elastomer substrate has been applied to fabricate stretchable PMSC-arrays [140,144]. For instance, a biaxially stretchable PMSC-array was fabricated on a deformable substrate of soft thermoplastic copolyester (Ecoflex) with locally embedded PET films [140]. Because of the stiffness differences between Ecoflex and PET, the local strain of active device region (above PET films) could be suppressed. As verified by finite element models, the maximum strain of PMSC region was  $\sim 0.02\%$  under 50% biaxial stretching, while that on PET films was up to 260% (Fig. 6g and k). With CNT-based microelectrodes, ionogel electrolyte of poly(ethylene glycol) diacrylate/1-ethyl-3-methylimidazolium bis(trifluoromethylsulfonyl)imide (PEGDA/EMIMTFSI), and liquid metal (Galinstan) interconnection, the formed PMSC-arrays delivered a volumetric energy density of  $25 \text{ mW h cm}^{-3}$  and outstanding electrochemical stability under 100% uniaxial and 50% biaxial stretching. These studies indicate that the stretchable interconnect, substrate and encapsulation structures are extremely important for building mechanically robust PMSC-arrays.

### 3.3. Shapeless PMSCs

Recently, the shapeless PMSCs receive considerable attention for flexible and morphable electronics. To achieve shapeless PMSCs, the major challenge is to prevent the delamination of elec-

trodes from the substrates during erratic deformation. One obvious way is to encapsulate PMSC units using polymers for protection. However, this strategy would significantly increase the thickness and weight of inactive components in the PMSCs. To tackle this issue, Pal et al. [145] reported an innovative strategy of bonding the microelectrodes to the silk substrate for flexible and degradable PMSCs (Fig. 7a). Significantly, PH1000-silk protein composite could be further tuned by doping with rGO for achieving higher performance of PMSCs. Although the functionality under extreme deformation was not reported, it is reasonably assumed that this strategy would be effective in achieving shapeless PMSCs. Then, our group developed ultrathin shapeless MSCs (defined as SMSCs) by encapsulating MXene-based interdigital microelectrodes in GO-containing aqueous hydrogel electrolyte (GPAH) employing chemically cross-linked PVA/H<sub>2</sub>SO<sub>4</sub> (Fig. 7b and c) [146]. The unique substrate-free architecture greatly reduced the thickness and weight of the overall PMSCs. It is noted that GO served as ionic conductor, capacitance enhancer and water retainer to remarkably enhance the electrochemical performance of SMSCs. Consequently, the SMSCs exhibited ultrathin thickness of  $\sim 37 \mu\text{m}$  for overall device, superior areal capacitance of  $40.8 \text{ mF cm}^{-2}$ , and excellent mechanical flexibility upon extreme deformation (Fig. 7d), demonstrating coexistence of ultra-flexibility with high electrochemical performance. The SMSCs could be passed through a nozzle ten times smaller than its resting volume without any visible damage to the electrodes (Fig. 7e), exemplifying the shapeless characteristic. Furthermore, three serially-connected SMSCs presented unprecedented flexibility of  $\sim 100\%$  capacitance retention after 3000 crumpling cycles, manifesting good scalability and practicality of this protocol. Currently, the research in this direction is still at an early stage and truly shapeless PMSCs with all-quasi-solid components are yet to be realized. It is speculated that such new-concept PMSCs can be used to build shape-shifting smart microsystems, such as military reconnaissance, intelligent nanorobots, body implants, and targeted drug delivery.

To sum up, various flexible and stretchable PMSCs including few shapeless PMSCs have been developing rapidly at the stage of laboratory. To further improve their mechanical tolerance, the electrode materials, microelectrode structures, electrolytes, substrates, encapsulation and fabrication strategies all should be taken into account. In addition, the practical applications in modern microelectronics of flexible, stretchable and shapeless PMSCs are urgently needed, which will make our life more convenient and efficient.

## 4. Stimuli-responsive PMSCs

Apart from the above functions, stimuli-responsive capabilities are being introduced into PMSCs for enriching their functionalities and in-situ monitoring the physical/chemical changes from internal or external environments [119,147,148]. So far, a series of smart PMSCs including self-healing [149–152], electrochromic [153–155], photo-responsive [156], and thermal-responsive devices [157,158] have been reported, showing tremendous prospect in the fields of intelligent electronics.

### 4.1. Self-healing PMSCs

The intended use of PMSCs is such that they will be subjected to various mechanical damage from outside source, which will seriously affect their electrochemical performance and lead to a collapse of the entire equipment [148]. Therefore, self-healing ability and ductility are necessary for PMSCs to self-repair internal or external damage. However, self-healing PMSCs are usually limited to low healing efficiency and circulatory nature (no more than 5) [159]. To address these issues, extensive efforts are being

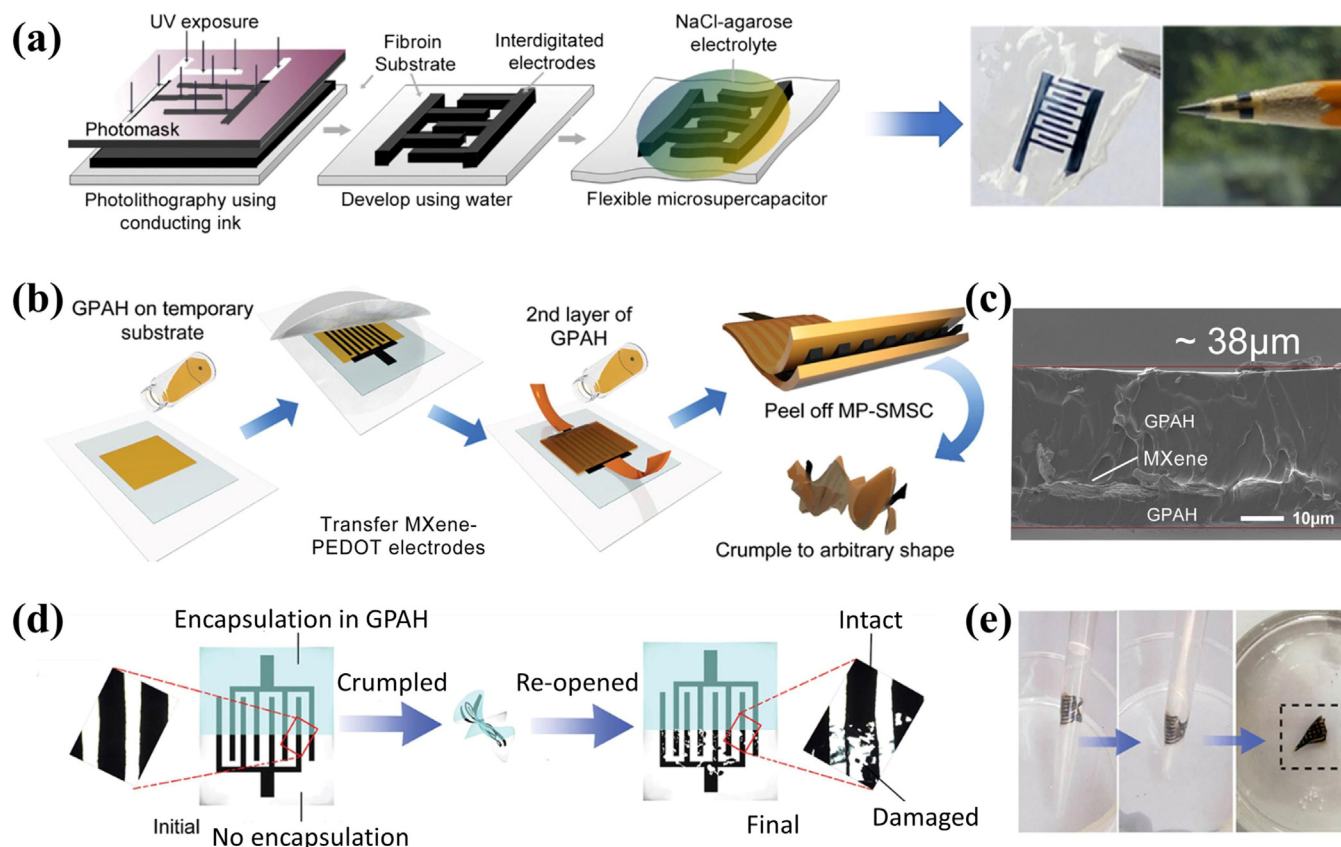


**Fig. 7.** Shapeless PMSCs. (a) Schematic showing the strategy for constructing flexible and degradable PMSCs. Reproduced with permission from Ref. [145], Copyright 2018, American Chemical Society. (b) Scheme of the fabrication of interdigital SMSCs. (c) SEM image of ultrathin-film microelectrode encapsulated within GPAH, (d) optical microscopy image showing the protective role of the hydrogel electrolyte (upper section) compared to the severe microstructural damage in the unencapsulated region (lower region), and (e) demonstration of shapeless characteristics of an SMSC by passing it through a fluid channel completely unharmed. Reproduced with permission from Ref. [146], Copyright 2021, Wiley-VCH.

devoted to improving self-healing ability of electrode materials and importing self-healing properties into electrolytes/substrates [149–152].

As a representative example, Yue et al. [149] developed a self-healing PMSC using polyurethane (PU)-coated  $\text{Ti}_3\text{C}_2\text{T}_x$ -rGO aerogel as electrode and PVA/ $\text{H}_2\text{SO}_4$  as gel electrolyte (Fig. 8a). Through integrating the good conductivity and high capacitance of  $\text{Ti}_3\text{C}_2\text{T}_x$ -rGO electrode with superior self-healing feature of carboxylated PU shell, the PMSC exhibited an areal capacitance of  $34.6 \text{ mF cm}^{-2}$ , outstanding cycling stability of 91% retention for 15,000 cycles, good self-healing property with 81.7% retention after the fifth repairing. This work testified that self-healing materials applied in PMSCs could effectively restore the electrochemical performance and structural integrity of damaged microdevices. In addition, self-healing polymers are favored by researchers to construct self-healing electrolytes of PMSCs. Recently, Shi et al. [150] reported PMSCs with a self-healable and stretchable ionogel electrolyte (Fig. 8b). Notably, the ionogel electrolyte was designed with a double-dynamic network consisting of metal-ligand crosslinked PEO- $\text{Li}^+$  and elastic hydrogen bond crosslinked polyethylene oxide-poly(propylene oxide)-poly(ethylene oxide) (PEO-PPO-PEO), thus delivering a tensile fracture strength of 0.96 MPa, high stretchability of  $\sim 1847\%$ , and superior electrochemical stability. Then, these PMSCs based on CNT electrodes could retain 98% capacitance after 2 min and five cutting/healing cycles (Fig. 8c), and exhibit maximum energy density of  $81.88 \text{ } \mu\text{W h cm}^{-2}$  at  $0.75 \text{ mW cm}^{-2}$ . These two studies provide fascinating directions for designing self-healable substrate, electrode and electrolyte for the next-generation self-healing devices.

#### 4.2. Electrochromic PMSCs

Electrochromism refers to a reversible color change of device under different operating voltage, which is derived from the electrochemical reduction/oxidation reactions of electrode [160,161]. By importing electrochromic functionality, the PMSCs can visually monitor their charging and discharging statuses and ensure their normal operation in real-time. So far, the usage of electrochromic materials as active electrode or electrolyte additive has been demonstrated in electrochromic PMSCs, endowing the double function of energy storage and visual indication of energy storage level [153–155].

Because of variable color and high pseudocapacitance, metal oxides and conductive polymers are deemed common electrochromic materials as active electrodes of electrochromic PMSCs [161,162]. For example, Qin et al. [153] reported an electrochromic PMSC-array with interdigital microelectrodes of Ag nanowires/NiO and gel electrolyte of PVA/KOH (Fig. 8d). According to the reversible reaction of  $\text{NiO} + \text{OH}^- \rightleftharpoons \text{NiOOH} + \text{e}^-$ , the positive electrodes of electrochromic PMSC showed gray color when it was charged to 0.5 V, and turned darker upon charging to 1.0 V. Meanwhile, the negative electrode remained transparent during the whole charging process. Moreover, the single PMSC exhibited distinct redox peaks between 0 to 1.0 V, maximal areal capacitance of  $3.47 \text{ mF cm}^{-2}$ , and impressive cycling stability of 80.7% retention for 10,000 cycles, indicative of superior energy storage ability. Finally, a smart self-charging integrated microsystem was constructed by integrating this electrochromic PMSC-array with hybrid tribo/piezoelectric nanogenerator, demonstrating suitable properties

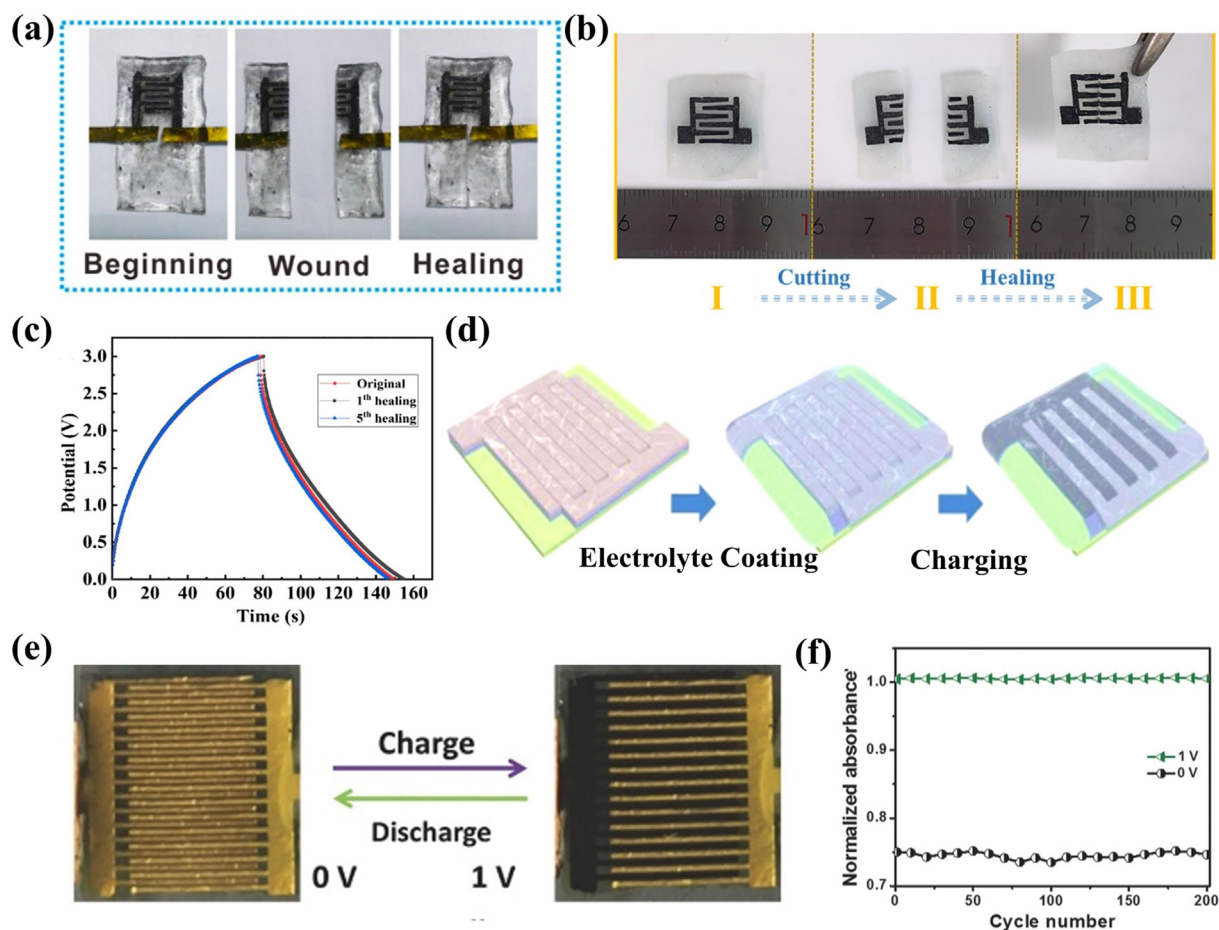


**Fig. 8.** Self-healing PMSCs and electrochromic PMSCs. (a) Optical images of self-healing  $\text{Ti}_3\text{C}_2\text{T}_x\text{-rGO}$  based PMSCs under original, cutting and self-healing states. Reproduced with permission from Ref. [149], Copyright 2018, American Chemical Society. (b) Photographs under different states, and (c) GCD profiles obtained at pristine, 1st self-healing and 5th self-healing states of PMSCs with self-healable ionogel electrolyte. Reproduced with permission from Ref. [150], Copyright 2020, Elsevier. (d) Schematic illustration of electrochromic PMSCs with Ag nanowires/NiO electrode. Reproduced with permission from Ref. [153], Copyright 2018, Springer. (e) Photographs of the reversible electrochromic effect, and (f) electrochromic stability of 200 cycles for EG/ $\text{V}_2\text{O}_5$  based electrochromic PMSCs with viologen electrolyte additive. Reproduced with permission from Ref. [154], Copyright 2017, Wiley-VCH.

for detectable self-powered microsystems. In addition, the electrochromic PMSCs can be readily obtained by introducing electrochromic electrolyte additive [154,155]. For instance, Feng and coworkers developed electrochromic PMSCs with EG/ $\text{V}_2\text{O}_5$  as active electrode, PVA/LiCl as gel electrolyte and stimulus-responsive viologen as electrochromic additive (Fig. 8e) [154]. The resulting PMSCs displayed reversible electrochromic effect in the charging/discharging processes of 0–1.0 V, originating from the electrically driven equilibrium between the colorless viologen of  $\text{MV}^{2+}$  and purple viologen derivative of  $\text{MV}^+$ . The in-situ ultraviolet (UV)-vis spectra further confirmed impressive electrochromic stability of PMSCs for 200 cycles (Fig. 8f). Also, the electrochromic PMSCs revealed high energy density of  $20 \text{ mWh cm}^{-3}$  and power density of  $235 \text{ W cm}^{-3}$ , and a long lifetime of 93% capacitance retention after 6000 cycles. These findings illustrate that electrochromic PMSCs can pave ways for developing high-performance electronics with visualized energy levels.

#### 4.3. Photo-responsive PMSCs

Light is regarded as one of the most common external stimuli owing to its ubiquity, diversity, and high temporal and spatial resolution [163,164]. Therefore, photo-responsive PMSCs are of great significance for selectively powering other instruments according to the intensity of various light. However, the studies on photo-

responsive PMSCs have not matured yet. Leading the research in this direction, Liu et al. [156] proposed a photo-switchable PMSC in 2017, using the composite film electrode of photoisomerized 1,2-bis(2,4-dimethyl-5-phenyl-3-thienyl)-3,3,4,4,5,5-hexafluoro-1-cyclopentene (DAE) deposited on graphene (Fig. 9a). With PVA/ $\text{H}_2\text{SO}_4$  gel electrolyte, the PMSC could operate at a high scan rate of  $10^4 \text{ V s}^{-1}$ , corresponding to an ultra-short charge–discharge time of 0.2 ms. Owing to reversible photoisomerization of DAE in UV and visible lights, the capacitance of as-fabricated PMSCs rapidly increased to 120% of original value once the device was exposed to UV light (Fig. 9b). Then, the capacitance recovered under white light irradiation, verifying the photo-switching ability of DAE-graphene based PMSC and disclosing the reversible shift of charge equilibrium at DAE-graphene interface. This underrated area of electronics deserves substantially more efforts to achieve novel high-sensitive photo-responsive PMSCs for noncontact tunable microelectronics.

#### 4.4. Thermal-responsive PMSCs

Due to the small space and high power delivery, PMSCs usually suffer thermal runaway problems, resulting in decreased lifespan and underlying security hazards [43,165]. Thus, rational design of thermal-control PMSCs is particularly important for the development of safe and high-performance on-chip electronics [148,166].

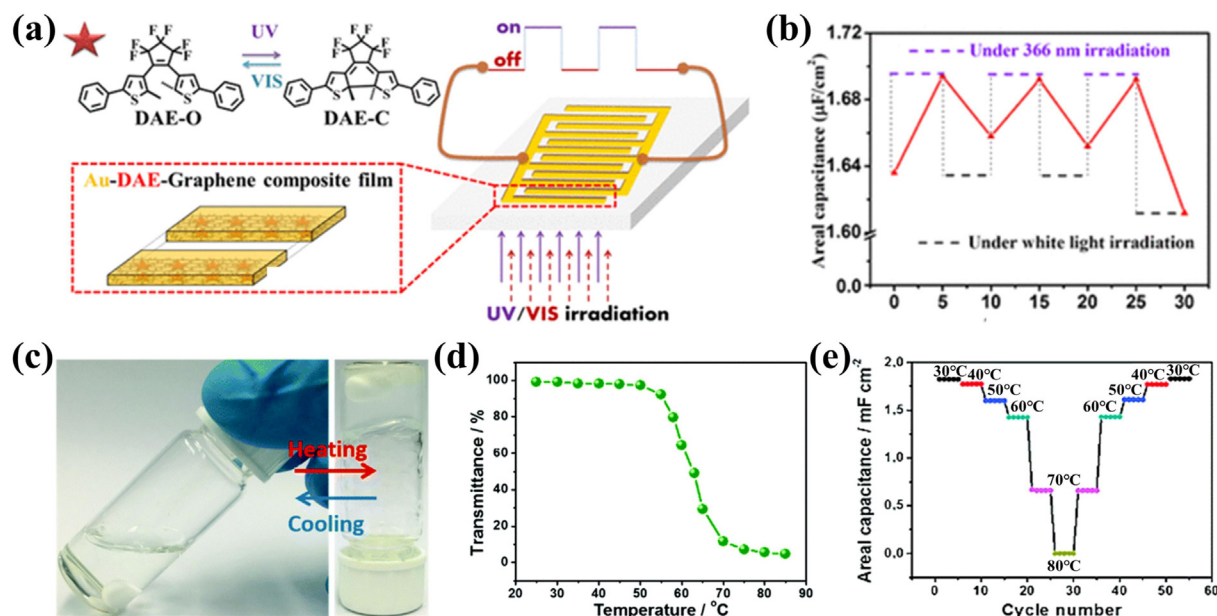


**Fig. 9.** Photo-responsive PMSCs and thermal-responsive PMSCs. (a) Schematic illustration, and (b) on-off switching behavior of photo-switchable PMSCs with DAE-graphene electrode in UV and visible lights. Reproduced with permission from Ref. [156], Copyright 2017, American Chemical Society. (c) Photographs of reversible sol-gel transition, and (d) transmittance versus temperature for PNIPAAm/MC/LiCl electrolyte under 30–80 °C, (e) areal capacitance of TS-MSC versus temperature. Reproduced with permission from Ref. [157], Copyright 2018, Royal Society of Chemistry.

Recently, adding thermal-responsive materials into electrolyte has become an effective strategy to sensitively sense ambient thermal risk and reversibly control the operation of PMSCs [157,158]. For example, Zhang et al. [157] developed a thermo-switchable PMSC (TS-MSC) based on the thermodynamic behavior of poly(*N*-isopropylacrylamide)-*g*-methylcellulose with 0.1 M LiCl (PNIPAAm/MC/LiCl) sol electrolyte (Fig. 9c). Using PEDOT film as active electrode, the TS-MSC offered an areal capacitance of 2.4 mF cm<sup>-2</sup>, volumetric capacitance of 25 ± 5 F cm<sup>-3</sup> at 20 μA cm<sup>-2</sup>, and good cycling stability of 88% retention over 5000 cycles. Moreover, the reversible change of ionic conductivity of PNIPAAm/MC/LiCl electrolyte enabled TS-MSC with 100% switch-off of the capacitance at 80 °C (Fig. 9d). After cooling to room temperature, the capacitance of TS-MSC could be fully recovered. And upon 50 heating-cooling cycles, almost no decay was observed for TS-MSC, implying its excellent reversibility (Fig. 9e). Furthermore, Zhang et al. [158] put forward another thermal-responsive material (Pluronic/PNI-PAM/AM) with *N*-isopropylacrylamide (NIPAM) as thermal-responsive unit, acrylamide (AM) as hydrophilic component and PEO-PPO-PEO (Pluronic) as polymer backbone. The Pluronic/PNI-PAM/AM grafted copolymer exhibited highly reversible sol-gel transition under 25–80 °C. Once dissolved in 0.5 M H<sub>3</sub>PO<sub>4</sub> or LiNO<sub>3</sub> aqueous solution, a thermo-reversible electrolyte was obtained to assemble carbon-based PMSCs. As a result, the thermal-responsive PMSCs displayed 95% of capacitance loss and 1% of ionic conductivity retention upon going from 25 to 80 °C, and outstanding reversibility for 20 heating-cooling cycles. Therefore, these thermal-responsive electrolyte systems offer an attractive solution to fabricate self-protective PMSCs for new-generation microelectronics with enhanced safety.

The above-mentioned PMSCs effectively integrated energy storage capacity with stimulus-responsive functionality, which has improved their space utilization and expanded their breadth of potential application. Apart from self-healing, electrochromic, photo-responsive and thermal-responsive PMSCs, new response modes (e.g., PH, humidity, force and various gases) also have great scope for further development. Meanwhile, it is important to improve their sensitivity, response range and cycle stability upon

different stimuli without losing the electrochemical performance. This is possible by achieving a deeper understanding of the effect mechanism through theoretical simulation and in-situ characterizations [167–170].

## 5. Other functional PMSCs

In addition to high-voltage, flexible/stretchable and stimuli-responsive PMSCs mentioned above, there are many other functional MSCs, such as transparent PMSCs [171–174], and alternating current line-filtering PMSCs [175–181].

Transparent PMSCs possess high optical transmittance and outstanding energy storage capacity, making them one of the best choices for transparent electronic devices [171–174]. By virtue of atomic-scale thickness, large SSA, high transparency, admirable elasticity and tunable electrochemical performance, 2D materials (e.g., graphene, MoS<sub>2</sub>) have proven themselves as hopeful electrode materials for transparent PMSCs [182–185]. As a demonstration, Delekta et al. [171] developed transparent graphene-based PMSCs by a simple and effective inkjet printing strategy on rigid/flexible substrates (Fig. 10a–c). Significantly, the resulting PMSCs presented superior electrochemical performance versus transparency, e.g., an areal capacitance of 16 μF cm<sup>-2</sup> at the transmittance of 90%, and a capacitance of 99 μF cm<sup>-2</sup> at the transmittance of 71% (Fig. 10a). Moreover, the negligible capacitance decay under different radii bending confirmed good mechanical flexibility of as-fabricated transparent PMSCs on flexible glass (Fig. 10b and c). Afterwards, transparent PMSCs based on MoS<sub>2</sub> nanosheets and PH1000 have also been widely reported [172–174]. They could realize both high electrochemical performance and transparency of >75%, opening up new way for designing transparent PMSCs in transparent electronic fields.

Furthermore, with fast frequency response feature, PMSCs can replace bulky aluminum electrolytic capacitors (AECs) and work as alternating current line-filters to rectify pulsed energy input in the kilo Hertz (Hz) range [186,187]. So far, various alternating cur-

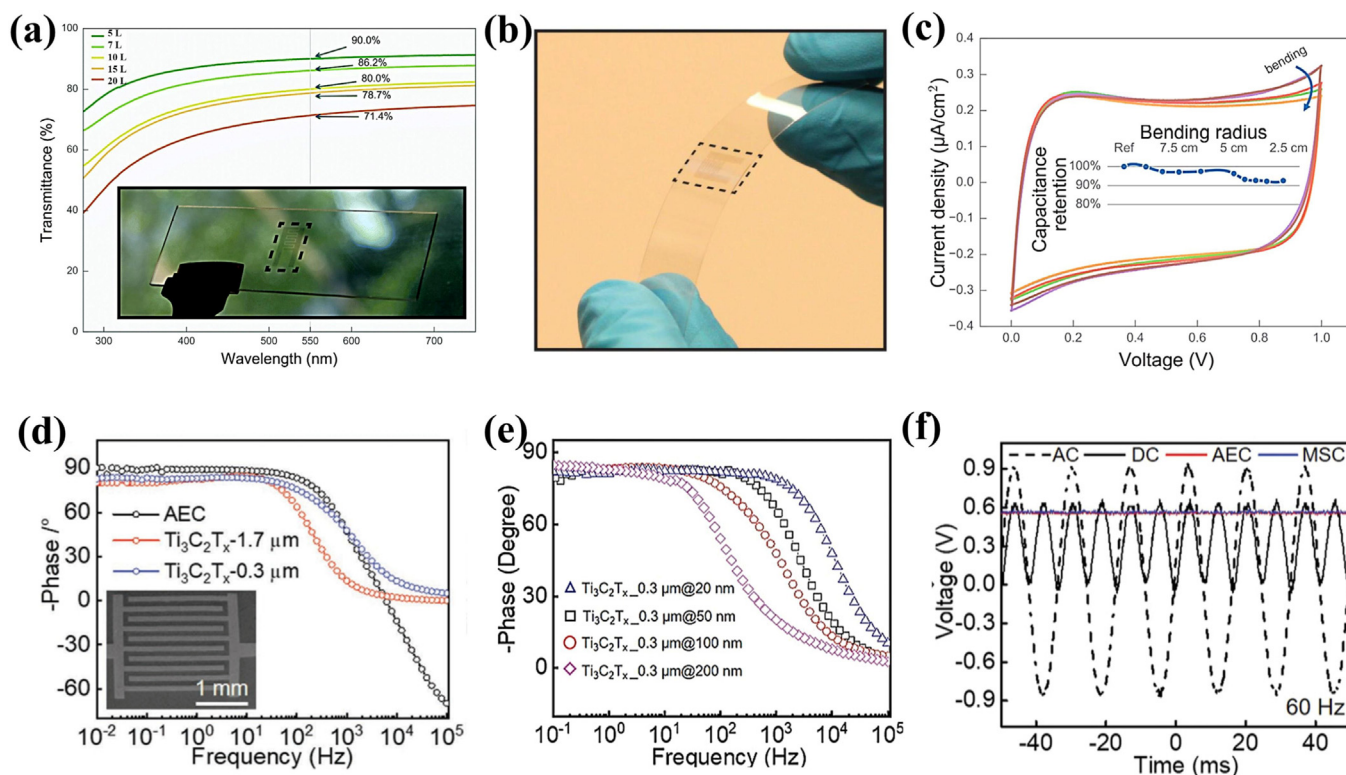


**Fig. 10.** Transparent PMSCs and alternating current line-filtering PMSCs. (a) Transmittance spectra of graphene electrode with different thickness, (b) optical photograph, and (c) CV curves under varying bending radii at  $50 \text{ mV s}^{-1}$  for flexible, transparent graphene-based PMSCs. Reproduced with permission from Ref. [171], Copyright 2017, Royal Society of Chemistry. (d, e) Alternating current line-filtering performance of MXene-based PMSCs with (d) different MXene sizes and (e) varying electrode thickness, (f) output voltage signals with MXene-based PMSCs and commercial AEC. Reproduced with permission from Ref. [175], Copyright 2019, Wiley-VCH.

rent line-filtering PMSCs have been developed, in which highly conductive active materials are recognized as the core to improve their filtering performance [175–181]. For instance, Alshareef and coworkers reported MXene-based PMSCs with tunable MXene sizes and engineered microelectrode designs for alternating current line-filtering applications [175]. The interdigital PMSCs with 100 nm thick microelectrodes and  $10 \mu\text{m}$  of finger spacing presented high capacitance of  $30 \text{ F cm}^{-3}$  at 120 Hz, outstanding rate capability up to  $300 \text{ V s}^{-1}$ , large negative phase angle of  $-76^\circ$  at 120 Hz (close to commercial AECs of  $-84^\circ$ ), and ultrashort relaxation time constant of 0.45 ms (Fig. 10d and e). As demonstrated, the PMSCs could efficiently convert alternating current signal with a peak voltage of 0.6 V to a constant voltage of  $\sim 0.56 \text{ V}$ , verifying high-efficiency filtering of voltage ripples (Fig. 10f). Hence, alternating current line-filtering PMSCs simultaneously achieved capacitance and ripple filtering, are able to accelerate the progress of next-generation MESDs for self-powered integrated microsystems.

The representative electrochemical performance metrics of various reported functional PMSCs have been summarized in Table S1 for better clarity. In the near future, we firmly believe that more functional PMSCs (such as self-charging, biocompatible and biodegradable devices) will be developed and applied to different application scenarios.

## 6. Smart PMSC-integrated microsystems

Constructing self-powered integrated microsystems on chip is the ultimate goal of designing various PMSCs, in which the PMSCs as energy storage parts are coupled with energy harvesters (e.g., solar cells and nanogenerators) [188–191] and energy consump-

tion units (e.g., different sensors and photodetectors) [192–195]. Conventionally, most PMSCs have acted as independent units and powered smart electronics with bulky external connections, resulting in increased size and energy expenditure [2,17,196]. Therefore, the on-chip fabrication of energy harvester-PMSC or PMSC-energy consumption integrated microsystem, and even all-in-one self-powered microsystem is considered an effective strategy for gaining advanced modern electronics with high compatibility and processability.

### 6.1. Energy harvester-PMSC integrated microsystem

Triboelectric/piezoelectric nanogenerators [191,197,198], photocatalytic fuel cells (PFCs) [199,200] and solar cells [190,201] are representative energy harvesters, which can effectively convert mechanical, biofuel and solar energy into electricity. When these energy harvesters integrate with energy storage PMSCs, a self-charging power unit can be obtained. As an example, Jiang et al. [202] developed a wearable and flexible energy harvester-PMSC integrated microsystem by coupling triboelectric nanogenerator (TENG) with MXene-based PMSCs (Fig. 11a). Specifically, the electricity was produced from the mechanical energy of human biomechanical motions using TENG, and then stored in high-performance MXene-based PMSCs. As demonstrated, the integrated microsystem could constantly charge during normal human motion ( $\sim 5 \text{ Hz}$ ) with ignorable current leakage, and subsequently power a digital watch or temperature-humidity meter. Besides, hybrid piezo/triboelectric nanogenerators were exploited to integrate with electrochromic PMSCs (positive electrode being transparent at 0 V, gray at 0.5 V and dark at 1.0 V, Fig. 11b) [153]. Interestingly, the hybrid nanogenerators exhibited high voltage output of 150 V

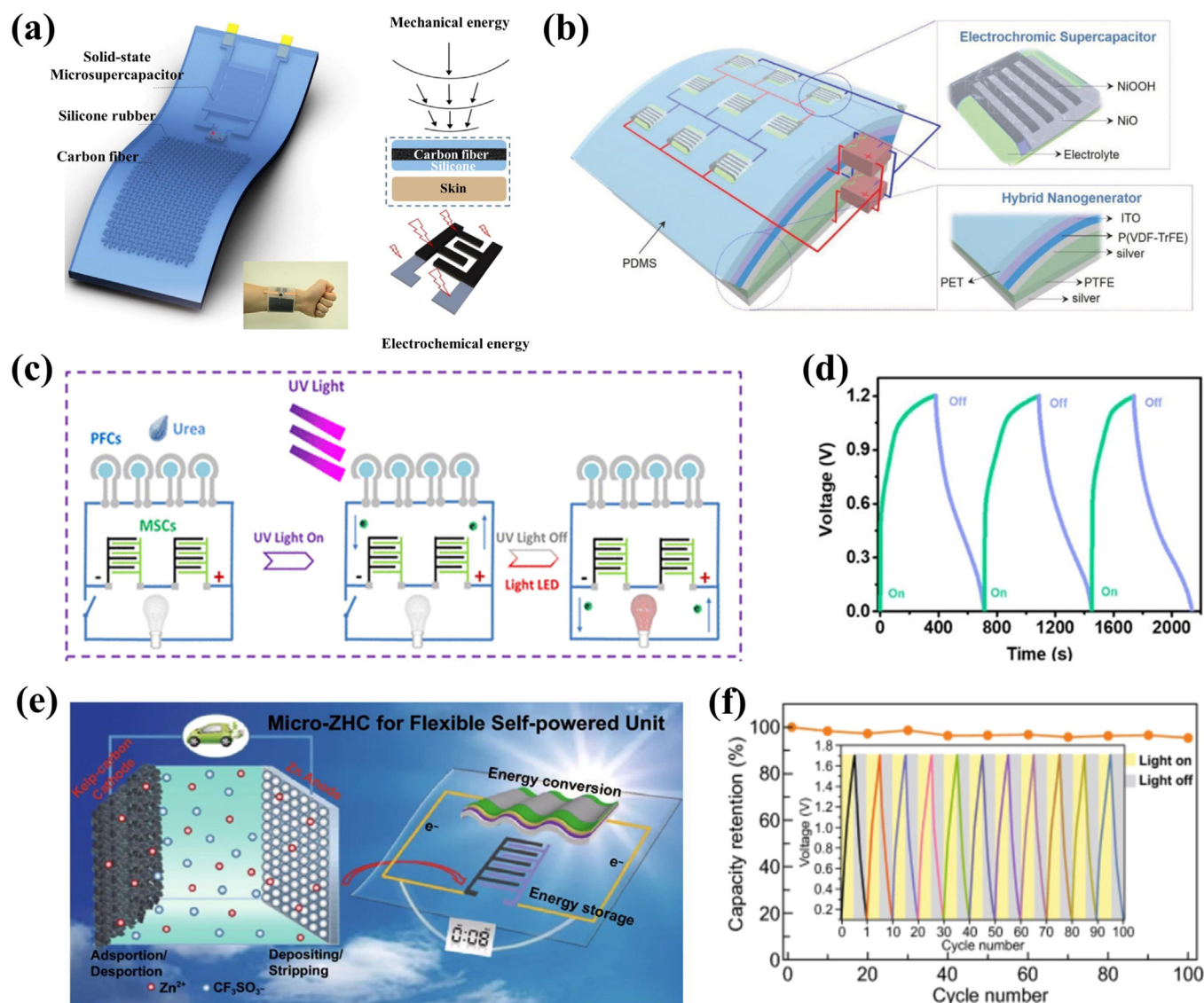


**Fig. 11.** Energy harvester-PMSC integrated microsystems. (a) Schematic diagram of TENG-PMSC integrated microsystem. Reproduced with permission from Ref. [202], Copyright 2018, Elsevier. (b) Schematic illustration of the integrated microsystem of hybrid piezo/triboelectric nanogenerators and electrochromic PMSCs. Reproduced with permission from Ref. [153], Copyright 2018, Wiley-VCH. (c) Schematic of the flexible PFC-AMSC integrated microsystem, and (d) GCD profiles of the AMSCs powered by PFCs. Reproduced with permission from Ref. [200], Copyright 2019, American Chemical Society. (e) Graphical illustration of solar cell-Zn-MSCs integrated microsystem, and (f) cycling performance of Zn-MSCs driven by solar cells. Reproduced with permission from Ref. [79], Copyright 2020, Springer.

and current output of 20  $\mu\text{A}$ , endowing PMSCs with fast charging to 3 V and powering a light-emitting diode (LED). Finally, the self-charging integrated microsystem could judge the charge/discharge states of PMSCs under human palm impact in real-time, indicating the huge potential of nanogenerator-PMSC integrated microsystems for developing self-charging intelligent electronics.

In recent years, the integration of PFCs and solar cells with PMSCs has also been reported for fabricating self-charging energy collection-PMSC systems [79,200,203]. For instance, Qiu et al. [200] designed a flexible PFC-PMSC energy chip with environment friendly PFCs as energy harvesters and AMSCs as energy storage units on the same plane (Fig. 11c). Significantly, the AMSCs were composed of NiCoP@NiOOH positive electrode and zeolite imidazole framework derived carbon (ZIF-C) negative electrode, which demonstrated large areal capacitance of 54.7  $\text{mF cm}^{-2}$  and areal energy density of 13.9  $\mu\text{W h cm}^{-2}$  at 270.5  $\mu\text{W cm}^{-2}$ . Meanwhile, the PFCs were assembled with silver and  $\text{TiO}_2$  electrodes, showing an impressive power density of 3.04  $\mu\text{W cm}^{-2}$  in 1 M urea solution

under UV irradiation. In this PFC-AMSC integrated microsystem, once UV light was turned on and urea was added, the PFCs immediately charged the AMSCs with high voltage and current to effectively light up a LED for a few minutes. This process could also be repeated over a few cycles (Fig. 11d), illustrating the feasibility of PFC-AMSC system in portable electronic applications. In another case, a self-charging power system with printed Zn-MSCs as energy storage device and solar cells as energy collector module was demonstrated (Fig. 11e) [79]. The Zn-MSCs exhibited outstanding areal capacity (10.28  $\mu\text{A h cm}^{-2}$ ) and high energy density (8.2  $\mu\text{W h cm}^{-2}$ ). And the organic solar cells revealed high energy conversion/storage efficiency (17.8%) and rapid photoelectric conversion rate, enabling Zn-MSCs to be charged up to 1.6 V within 23 s. By the effective coupling of solar cells and Zn-MSCs in flexible PET substrate, the integrated microsystem displayed superior mechanical flexibility and cycling stability, e.g., 86% capacitance retention over 50 bending cycles at 120°, and 95% retention after 100 charge-discharge cycles (Fig. 11f). Such flexible energy

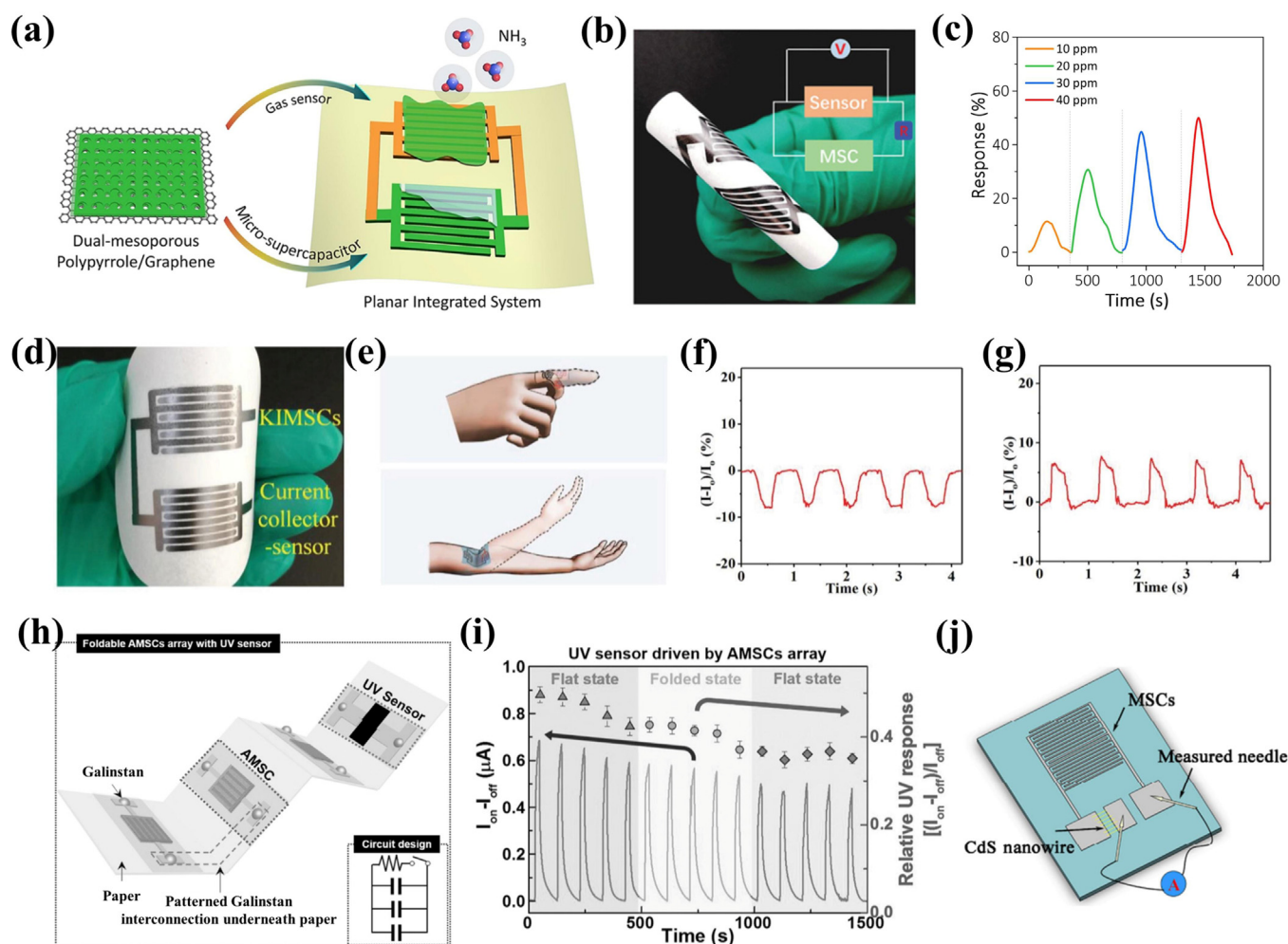


**Fig. 12.** PMSC-energy consumption integrated microsystems. (a) Schematic diagram, (b) optical picture and equivalent circuit of PMSC-NH<sub>3</sub> sensor integrated microsystem, and (c) response curves of NH<sub>3</sub> sensor powered by one DM-PG based PMSC. Reproduced with permission from Ref. [206], Copyright 2020, Wiley-VCH. (d) Photograph of K-MSC-pressure sensor integrated microsystem, (e) scheme illustrating the integrated microsystem on the finger and elbow, (f, g) current responses of graphene-based pressure sensor driven by a K-MSC upon (f) finger bending, and (g) elbow movement. Reproduced with permission from Ref. [88], Copyright 2021, Wiley-VCH. (h) Schematic illustration and equivalent circuit of AMSC-UV sensor integrated microsystem, and (i) UV response of graphene/ZnO-based UV sensor powered by AMSCs under repetitive folding cycles. Reproduced with permission from Ref. [90], Copyright 2017, Wiley-VCH. (j) Schematic of the PMSC-photodetector integrated microsystem. Reproduced with permission from Ref. [217], Copyright 2016, Springer.

harvester-PMSC integrated microsystems realize the possibility of designing highly safe, self-powered microsystems for advanced wearable electronics.

## 6.2. PMSC-energy consumption integrated microsystem

Similarly, fabricating an integrated microsystem of PMSCs with energy consumption (i.e., functional sensing/detecting units) has garnered extensive attention [194,204,205], because they can offer a real-time monitoring of physical, chemical and biological signals of human body or surrounding environment for managing physical health, controlling industrial production and reducing environmental pollution. Thus, diversified PMSC-energy consumption integrated microsystems including PMSC-gas sensor [206–210], PMSC-pressure sensor [88,211,212], PMSC-UV sensor [90,207,213–216] and PMSC-photodetecting systems [149,217,218], have been constructed in recent years.

Chemical gas sensors are crucial for monitoring air pollutants and noninvasive screening diagnosis [192,219]. To extend their applications into the portable and wearable operation, our group designed a new-concept PMSC-NH<sub>3</sub> sensor integrated microsystem based on bi-functional active materials of 2D dual-mesoporous

polypyrrole/graphene (DM-PG) in Fig. 12(a) [206]. DM-PG was rationally designed with ordered dual-mesopores of 7 and 18 nm, and exhibited both superior NH<sub>3</sub> response as low as 200 ppm and higher capacitance of 376 F g<sup>-1</sup>, outperforming their single-mesoporous and non-mesoporous counterparts. Moreover, the bi-functional DM-PG enabled PMSC-NH<sub>3</sub> sensor integrated microsystem quickly responding to NH<sub>3</sub> in concentration as low as 10–40 ppm after charging for only 100 s (Fig. 12b and c). At various bending angles, the integrated microsystem could work steadily and delivered 82% response retention at 180°, indicative of favorable flexibility. This work opens up the attractive opportunities in designing multifunctional materials for integrated microsystems with high compatibility.

Among physical sensors, pressure sensors are important as they can collect mechanical data of human body or surroundings and convert them into electrical signals for monitoring physiological health [194,220]. In this regard, some PMSC-pressure sensor integrated microsystems have been demonstrated for realizing wireless operation [88,211,212]. As a prime example, Zheng et al. [88] developed a high-performance integrated microsystem with high-voltage K-MSC (3.8 V) and graphene-based pressure sensor by mask-assisted filtration technique (Fig. 12d). It is noted that

K-MSC revealed energy density of  $34.1 \text{ mW h cm}^{-3}$  and low self-discharge with 44 h from 3.8 to 2.4 V. As a result, the K-MSC-pressure sensor microsystem presented sensitive response to body motions, e.g.,  $\sim 8\%$  response variation for finger bending, and  $\sim 7\%$  response variation over elbow movement (Fig. 12e–g). It was verified that PMSC-pressure sensor systems show great sensitivity in recording body motions, taking a positive step towards smart wearable electronics.

In line with general health monitoring, the detection of UV rays and protection from UV rays in day-to-day life are also of great significance. Inspired by this, various PMSC-UV sensor integrated microsystems have been constructed recently [90,207,213–216]. For example, Yun et al. [90] reported a foldable integrated array of three AMSCs and one graphene/ZnO-based UV sensor on a paper substrate (Fig. 12h). Notably, the AMSCs were composed of  $\text{MnO}_2/\text{CNT}$  positive electrode,  $\text{V}_2\text{O}_5/\text{CNT}$  negative electrode and organic gel electrolyte of PC-poly(methyl methacrylate) (PMMA)- $\text{LiClO}_4$ . Due to excellent electrochemical performance, e.g., 1.6 V of voltage window and  $0.88 \mu\text{Wh cm}^{-2}$  of energy density, three parallelly-connected AMSCs could steadily drive the graphene/ZnO-based UV sensor. As proved in Fig. 12(i), the as-fabricated AMSC-UV sensor integrated microsystem could effectively detect UV rays for 1500 s under repetitive folding cycles, demonstrating its huge potential in flexible and foldable microelectronics.

Furthermore, photodetectors can integrate with PMSCs to build self-powered detector microsystems [149,217,218]. Typically, a PMSC-photodetector integrated microsystem consisting of one rGO/ $\text{Fe}_2\text{O}_3$ -based PMSC and one CdS-based photodetector was reported (Fig. 12j) [217]. One current collector of PMSC and the middle square microelectrode served as two electrodes of CdS-based photodetector. Remarkably, the PMSC displayed an impressive energy density of  $1.61 \text{ mW h cm}^{-3}$ , a maximum power density of  $9.82 \text{ W cm}^{-3}$ , superior cycling stability of 92% retention over 32,000 cycles, and long self-discharge time of 21000 s from 1.0 to 0.24 V. Driven by this high-performance PMSC, the photodetector revealed high sensitivity and good reproducibility under white light, e.g., a current on/off ratio of 10.53, short response and recovery times of 1.21 and 1.40 s, and linearly increasing photocurrent with varying light intensities, which are well comparable to the photodetector powered by external energy storage devices. These results indicated the feasibility of PMSC-photodetector integrated microsystems to replace traditional detection devices connected to the external power supply.

### 6.3. All-in-one self-powered microsystem

To realize truly wireless and self-powered units, integrating energy harvester, PMSCs and consumption devices into all-in-one self-powered microsystem on one substrate is crucial yet challenging. In recent years, a few planar self-powered microsystems have been developed, in which the energy harvester, PMSCs and energy consumption are connected with metallic interconnects or external wires [221–226]. For instance, Yun et al. [221] reported a stretchable self-powered array made up of commercial Si-based solar cells, PPy/CNT-based PMSCs and graphene foam-based strain sensor on one deformable polymer substrate (Fig. 13a). Specifically, the PMSCs with gel electrolyte of PVA/LiCl and 1-methyl-3-propylimidazolium iodide (MPII) redox additive exhibited maximum areal energy and power densities of  $0.44 \mu\text{W h cm}^{-2}$  and  $176.5 \mu\text{W cm}^{-2}$ , respectively. After combining twelve parallelly-connected PMSCs, two serially-connected solar cells and a strain sensor via serpentine metal interconnections (Ti/Pt film), the self-powered microsystem was achieved. As displayed in Fig. 13(b and c), the resulting microsystem could be attached to the wrist and delivered a uniform pulse signal of 15 beats per 10 s under sunlight. Moreover, the self-powered microsystem dis-

played sensitive response to the wrist motion, implying its potential in skin-attachable health-monitoring devices. In another work, a smart self-powered microsystem with a foldable Au-based TENG, ZnP nanosheet@laser-induced graphene foam (ZnP@LIG)-based PMSCs, and one crumpled graphene-based strain sensor was demonstrated (Fig. 13d), exhibiting stable voltage and power outputs, high energy storage capability, and sensitive response to applied strains [224]. However, the usage of complicated external wires and additional rectifier impeded the practical application of this self-powered microsystem in on-chip electronics. Recently, our group developed a planar all-in-one self-powered microsystem with Si-based photovoltaics (Si-PVs), graphene-CNT (GC)-based PMSC, and dual channel gas sensors on one flexible PET substrate (Fig. 13e) [225]. Remarkably, the self-powered microsystem showed impressive compatibility and good flexibility, attributed to the effective assembly of microelectrodes and non-metallic interconnects of PMSC and gas sensors in one step. Ultimately, the self-powered microsystem revealed high selectivity to  $\text{NH}_3$  and aniline of 25–100 ppm, good reproducibility to 75 ppm of  $\text{NH}_3$  or aniline for 5 cycles, and exceptional mechanical flexibility under different bending angles (Fig. 13f and g). However, the interconnects between flexible planar Si-PVs and PMSCs were copper tapes, and their seamless connection would further improve the application prospects.

A summary and comparison of electrochemical performance of these three PMSC-based integrated microsystems is presented in Table S1. In short, the full integration of energy harvester, PMSC and energy consumption on single substrate without external components is recognized as one real all-in-one self-powered microsystem. Nevertheless, there remains plenty of room for further innovation and optimization. In particular, simplified construction of different functional microelectronics and various interconnects in a limited space on one planar substrate would be an effective strategy for realizing true all-in-one self-powered microsystems.

## 7. Summary and perspective

Inspired by next-generation microelectronics, multifunctional PMSCs combining energy storage with other function (like high-voltage, flexibility/stretchability, and various stimuli-response), and PMSC-based integrated microsystems (including energy harvester-PMSC, PMSC-energy consumption and all-in-one self-powered devices) have developed rapidly. In principle, the device configuration, design strategies, energy storage capacity, and basic function mechanisms of high-voltage, flexible, stretchable, self-healing, electrochromic, photo-responsive and thermal-responsive PMSCs are elaborately discussed. Although these multifunctional PMSCs have their strengths and uniqueness, high-voltage and flexible devices are considered more important and promising, due to the synergistically improved output voltage and energy density, and the commercial demand of portable and wearable microelectronics, respectively. Meanwhile, ultrahigh-voltage modular integration, shapeless, transparent and alternating current line-filtering PMSCs have been innovatively proposed and show great impacts on the entire energy storage field. Further, the effective coupling of PMSCs with nanogenerators or solar cells, the direct utilization of PMSCs to power different sensors or photodetectors, and the full integration of energy harvester, PMSCs and energy consumption, have been presented to demonstrate the forthcoming self-powered integrated microsystems. In particular, realizing all-in-one self-powered microsystems is the ultimate goal of designing various PMSCs and PMSC-integrated systems, which can guide the future direction for advanced microelectronics. Despite gigantic achievements, several existing key challenges

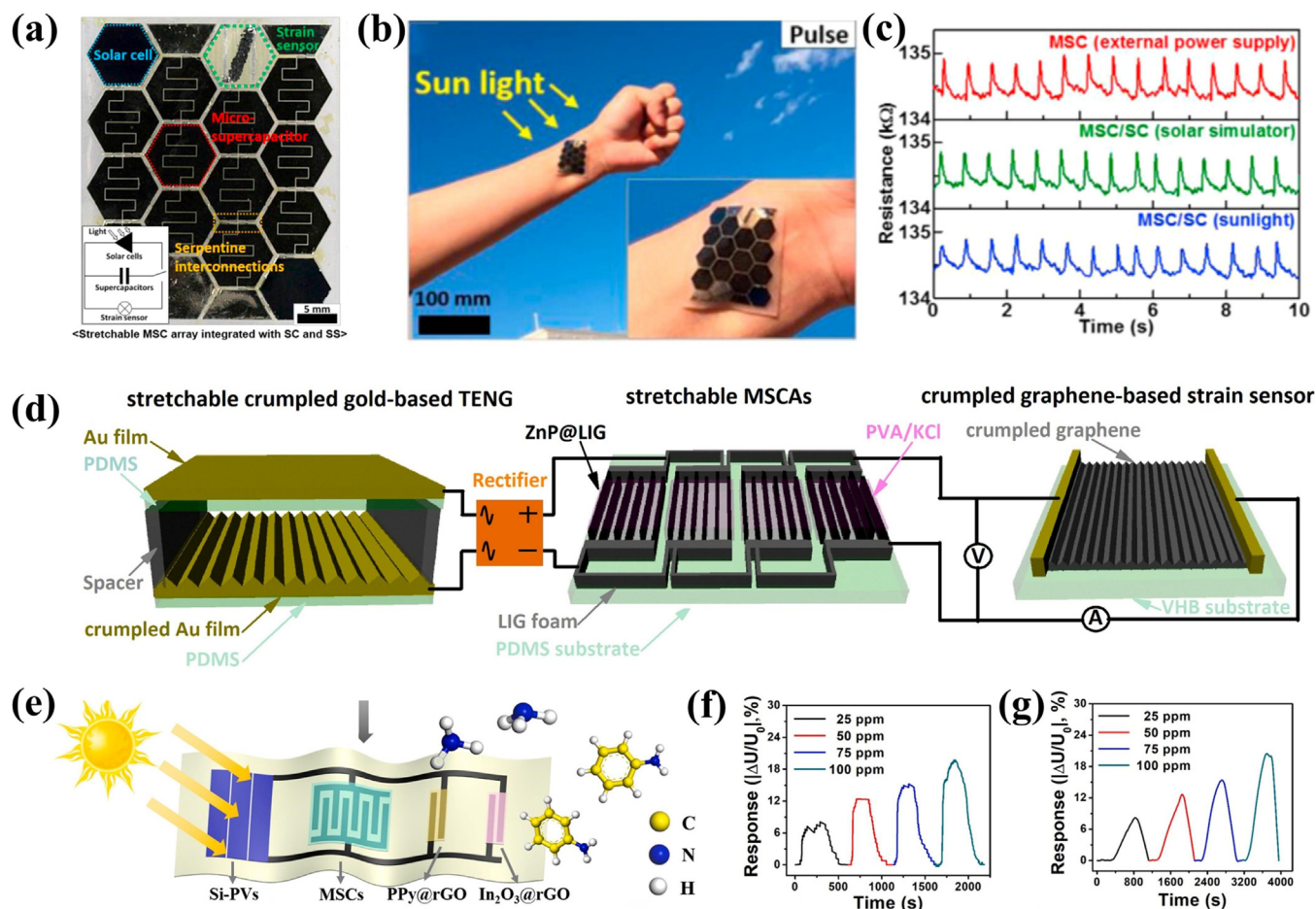


**Fig. 13.** All-in-one self-powered microsystems. (a) Optical image and equivalent circuit of the stretchable self-powered microsystem with solar cells, PMSCs and strain sensor, (b) photograph of the stretchable self-powered array attached to the skin, and (c) responses of the strain sensor driven by PMSCs charged with external power supply, solar simulator and solar light. Reproduced with permission from Ref. [221], Copyright 2018, Elsevier. (d) Schematic illustration of the smart self-powered microsystem with Au-based TENG, ZnP@LIG-based PMSC, and crumpled graphene-based strain sensor. Reproduced with permission from Ref. [224], Copyright 2021, Elsevier. (e) Schematic diagram of all-in-one self-powered microsystem with Si-PVs, PMSC and dual channel gas sensors, and (f, g) response curves towards (f) NH<sub>3</sub> and (g) aniline of the self-powered microsystem. Reproduced with permission from Ref. [225], Copyright 2021, Elsevier.

should be addressed in the future development of functional PMSCs and integrated microsystems.

#### (1) Designing multifunctional materials and microdevices

Multifunctional materials and microdevices with two or more functions for PMSCs and related integrated microsystems are crucial yet undeveloped. From the point of materials, most reported functional PMSCs are fabricated with multiple monofunctional materials, and the complicated preparation and poor compatibility severely hinder their practical application in potable, wearable and implantable microelectronics. Thus, designing multifunctional materials will be an effective strategy to accommodate fast and large-scale fabrication of functional PMSCs. Specifically, machine learning and high throughput simulation can be used to efficiently screen the multifunctional materials, providing the much-needed accurate predictions with accelerated research process and reduced trial-and-error costs. And the combination of theoretical and experimental analyses is equally important. For example, the heterostructure and composite materials can fully combine the advantages of individual materials and eliminate their drawbacks, thus enabling them with multiple functionalities in theory. As evidenced, the DM-PG heterostructures exhibited bi-functional features of sensitive response for NH<sub>3</sub> sensors and high capacitance

for PMSCs, deriving from the synergistic coupling of highly sensitive, pseudocapacitive PPy and high-conductive graphene [206]. Further, the bi-functional DM-PG enables a high-performance MSC-sensor integrated microsystem. From the perspective of microdevices, the architectural design of multifunctional PMSCs and their integrated microsystems should be paid much attention. Both mixing various monofunctional materials into a single electrode and introducing stimuli-responsive polymers or other organic/inorganic additives into the electrolyte could be possible avenues for realizing PMSCs with various specific requirements in a limited footprint. However, the compatibility of these functional components should be carefully taken into consideration to avoid importing complicated microfabrication process and weakening energy storage performance of multifunctional PMSCs.

#### (2) Developing advanced microfabrication techniques

For PMSCs, diverse microfabrication techniques have been developed to build customized microelectrodes [42,118,227], e.g., photolithography, laser processing, plasma etching, electrochemical deposition, inkjet printing, screen printing, and 3D printing. Although each technology possesses its own strengths and weaknesses, 3D printing has come to the forefront as a scalable and readily-available method for continuous large-scale production of

PMSCs, including microelectrodes, electrolytes and encapsulations in recent years [228,229]. For PMSC-based integrated microsystems, 3D printing also shows apparent advantages to realize their fabrication with reduced time, energy, and cost. However, a fully-printed self-powered microsystem is still at a theoretical stage due to the poor compatibility of each component and common requirement of complicated external circuit connections. Despite the ability of 3D printing technology to produce energy harvester (e.g., nanogenerators) [230,231], PMSCs [232], energy consumption (e.g., various sensors) [233,234] and electric interconnects individually, one-step construction and seamless connection of these units to fabricate energy harvester-PMSC-energy consumption microsystems are desperately needed for modern intelligent microelectronics.

### (3) Standardizing evaluation index of microdevices

Due to a lack of a unified and appropriate evaluation system, it is often difficult to compare the reported performance of microdevices and their integrated microsystems. Taking PMSCs as an example, the performance indicators are expressed in diverse forms by various units, such as mass/areal/volumetric capacitance, energy density and power density. Meanwhile, these performance parameters are calculated based on the mass/area/volume of microelectrodes with or without electrolyte and packaging. To fairly evaluate and compare the performance of PMSCs, establishing unified standards according to the application conditions is urgently needed. Apart from the energy storage performance, consistent functional indicators should also be provided for functional PMSCs. For example, flexible characteristics in terms of bending, twisting or stretching (including the degree, ultimate value, cycle numbers, stability after a certain cycle) have been widely used to describe and compare the flexibility of PMSCs. Considering the different application scenarios, the detailed and unified data (e.g., ultimate retention level and stability after a certain cycle) are crucial to uniformly contrast their comprehensive performance. For intelligent integrated microsystems, the elements are more complicated than single PMSCs, and no unified and effective evaluation system has been put forward so far. Therefore, the establishment of unified evaluation indexes from individual PMSCs to all-in-one self-powered microsystems needs close cooperation between researcher and large institutions to accomplish relevant standards step by step.

### (4) Balancing energy storage performance and functionality of functional PMSCs

Generally, the additional functions affect the intrinsic energy storage performance of functional PMSCs to a certain extent, including capacitance, energy density, power density and cycling stability. For high-voltage PMSCs, the output voltage and energy density can be synergistically improved by employing asymmetric configuration, high-voltage electrolyte, or self-integrating multiple devices without losing their power density and cycling stability. For flexible/stretchable PMSCs, their materials (including substrate, electrode, and electrolyte), structure and microfabrication all should be carefully taken into consideration to harmonize the relationship between energy storage performance and flexibility/stretchability. Obtaining deformable electrode structure, as well as selecting elastic substrate, interconnects and encapsulation is feasible to realize flexible/stretchable PMSCs with both high electrochemical performance and flexibility/stretchability. For stimuli-responsive PMSCs, introducing stimuli-responsive materials into microelectrode or electrolyte is regarded as a simple and efficient strategy. Nonetheless, the preparation of functional microelectrodes or electrolytes should match the working condi-

tion and device structure of stimuli-responsive PMSCs without sacrificing their energy storage performance. Only after a reliable balance between electrochemical performance and additional functions is achieved, ideal multifunctional devices can be fabricated for practical applications.

### (5) Realizing and applying real all-in-one self-powered microsystems

In terms of the final applications for intelligent microelectronics, it is critical and challenging to fabricate all-in-one self-powered microsystems with reduced size/space and compact integration on-chip. In view of this, various aspects including multifunctional compatible materials, advanced microfabrication technology, dense structure design and overall performance optimization should be considered. The elaborate design of multifunctional materials and efficient development of microfabrication techniques (e.g., 3D printing) for all-in-one self-powered microsystems have been discussed above in detail. For structure design, these units of energy harvester, PMSCs and energy consumption are expected to be coupled as closely as possible through pattern design, monolithic integration (both sides of substrate or stacked configuration), or seamless connection to enhance the space utilization. Further, optimizing the output voltage/current of energy harvester, the energy density and self-discharge property of PMSCs, sensitivity of energy consumption, and energy conversion efficiency between them are equally important. In addition, wireless technologies (e.g., near-field communications and Bluetooth) should be incorporated into PMSC-based integrated microsystems in order to transmit real-time data to external computers or telephones. With these continuous endeavors and an impetus in the directions discussed, it is believed that the truly all-in-one self-powered microsystems will be realized in near future for their practical applications and greatly promote the revolutionization of intelligent microelectronics in the coming era of 5G and Internet of Things.

### Declaration of competing interest

The authors declare that they have no known competing financial interests or personal relationships that could have appeared to influence the work reported in this paper.

### Acknowledgments

The authors acknowledge the National Natural Science Foundation of China, China (Grant Nos. 22125903, 51872283, 22109040), the “Transformational Technologies for Clean Energy and Demonstration” Strategic Priority Research Program of the Chinese Academy of Sciences (Grant No. XDA21000000), the Dalian Innovation Support Plan for High Level Talents, China (2019RT09), DICP, China (DICP I202032), the Dalian National Laboratory For Clean Energy (DNL), CAS, DNL Cooperation Fund, CAS, China (DNL202016, DNL202019), the Top-Notch Talent Program of Henan Agricultural University, China (30500947), and the Joint Fund of the Yulin University and the Dalian National Laboratory for Clean Energy, China (YLU-DNL Fund 2021002, YLU-DNL Fund 2021009).

### Appendix A. Supplementary material

Supplementary data to this article can be found online at <https://doi.org/10.1016/j.jechem.2023.01.065>.

### References

- [1] B. Dunn, H. Kamath, J.M. Tarascon, *Science* 334 (2011) 928–935.

- [2] P. Zhang, F. Wang, M. Yu, X. Zhuang, X. Feng, *Chem. Soc. Rev.* 47 (2018) 7426–7451.
- [3] S. Bi, H. Cao, R. Wang, F. Wan, Z. Niu, *J. Energy Chem.* 63 (2021) 25–39.
- [4] X. Shi, P. Das, Z.-S. Wu, *ACS Energy Lett.* 7 (2021) 267–281.
- [5] Y. Li, S. Xiao, T. Qiu, X. Lang, H. Tan, Y. Wang, Y. Li, *Energy Storage Mater.* 45 (2022) 741–767.
- [6] S. Zheng, X. Shi, P. Das, Z.-S. Wu, X. Bao, *Adv. Mater.* 31 (2019) 1900583.
- [7] C. Zhao, Y. Liu, S. Beirne, J. Razal, J. Chen, *Adv. Mater. Technol.* 3 (2018) 1800028.
- [8] J. Wang, F. Li, F. Zhu, O.G. Schmidt, *Small Methods* 3 (2019) 1800367.
- [9] S. Wang, J. Ma, X. Shi, Y. Zhu, Z.-S. Wu, *Nano Res. Energy* 1 (2022) e9120018.
- [10] F. Liu, X. Feng, Z.-S. Wu, *J. Energy Chem.* 76 (2023) 459–461.
- [11] F. Meng, Q. Li, L. Zheng, *Energy Storage Mater.* 8 (2017) 85–109.
- [12] D. Chen, K. Jiang, T. Huang, G. Shen, *Adv. Mater.* 32 (2020) e1901806.
- [13] H. Li, J. Liang, *Adv. Mater.* 32 (2020) e1805864.
- [14] J. Qin, P. Das, S. Zheng, Z.-S. Wu, *APL Mater.* 7 (2019).
- [15] C. Lethien, J. Le Bideau, T. Brousse, *Energy Environ. Sci.* 12 (2019) 96–115.
- [16] Z.-S. Wu, X.L. Feng, H.-M. Cheng, *Natl. Sci. Rev.* 1 (2014) 277–292.
- [17] B.D. Boruah, *Energy Storage Mater.* 21 (2019) 219–239.
- [18] J. Zhang, G. Zhang, T. Zhou, S. Sun, *Adv. Funct. Mater.* 30 (2020) 1910000.
- [19] G. Wang, L. Zhang, J. Zhang, *Chem. Soc. Rev.* 41 (2012) 797–828.
- [20] N. Liu, Y. Gao, *Small* 13 (2017) 1701989.
- [21] P. Simon, Y. Gogotsi, *Nat. Mater.* 19 (2020) 1151–1163.
- [22] Y. Zhai, Y. Dou, D. Zhao, P.F. Fulvio, R.T. Mayes, S. Dai, *Adv. Mater.* 23 (2011) 4828–4850.
- [23] D. Pech, M. Brunet, H. Durou, P. Huang, V. Mochalin, Y. Gogotsi, P.L. Taberna, P. Simon, *Nat. Nanotechnol.* 5 (2010) 651–654.
- [24] Q. Wang, J. Yan, Z. Fan, *Energy Environ. Sci.* 9 (2015) 729–762.
- [25] J. Liang, A.K. Mondal, D.W. Wang, F. Iacopi, *Adv. Mater. Technol.* 4 (2018) 1800200.
- [26] X. Shi, S. Zheng, Z.-S. Wu, X. Bao, *J. Energy Chem.* 27 (2018) 25–42.
- [27] Z. Pang, G. Li, X. Xiong, L. Ji, Q. Xu, X. Zou, X. Lu, *J. Energy Chem.* 61 (2021) 622–640.
- [28] V. Augustyn, P. Simon, B. Dunn, *Energy Environ. Sci.* 7 (2014) 1597–1614.
- [29] R. Chen, M. Yu, R.P. Sahu, I.K. Puri, I. Zhitomirsky, *Adv. Energy Mater.* 10 (2020) 1903848.
- [30] M. Kandasamy, S. Sahoo, S.K. Nayak, B. Chakraborty, C.S. Rout, *J. Mater. Chem. A* 9 (2021) 17643–17700.
- [31] Y. Shi, L. Peng, Y. Ding, Y. Zhao, G. Yu, *Chem. Soc. Rev.* 44 (2015) 6684–6696.
- [32] C. Zhao, X. Jia, K. Shu, C. Yu, G.G. Wallace, C. Wang, *J. Mater. Chem. A* 8 (2020) 4677–4699.
- [33] J. Ding, W. Hu, E. Paek, D. Mitlin, *Chem. Rev.* 118 (2018) 6457–6498.
- [34] A. Muzaffar, M.B. Ahmed, K. Deshmukh, J. Thirumalai, *Renew. Sust. Energy Rev.* 101 (2019) 123–145.
- [35] L. Xia, B. Tang, J. Wei, Z. Zhou, *Batteries Supercaps* 4 (2021) 1108–1121.
- [36] S. Zhang, N. Pan, *Adv. Energy Mater.* 5 (2015) 1401401.
- [37] Q. Wu, T. He, Y. Zhang, J. Zhang, Z. Wang, Y. Liu, L. Zhao, Y. Wu, F. Ran, *J. Mater. Chem. A* 9 (2021) 24094–24147.
- [38] Q. Jiang, Y. Lei, H. Liang, K. Xi, C. Xia, H.N. Alshareef, *Energy Storage Mater.* 27 (2020) 78–95.
- [39] M. Yu, X. Feng, *Joule* 3 (2019) 338–360.
- [40] R. Wang, M. Yao, Z. Niu, *InfoMat* 2 (2019) 113–125.
- [41] L. Liu, Z. Niu, J. Chen, *Nano Res.* 10 (2017) 1524–1544.
- [42] D. Qi, Y. Liu, Z. Liu, L. Zhang, X. Chen, *Adv. Mater.* 29 (2017) 1602802.
- [43] Y. Da, J. Liu, L. Zhou, X. Zhu, X. Chen, L. Fu, *Adv. Mater.* 31 (2019) e1802793.
- [44] F. Bu, W. Zhou, Y. Xu, Y. Du, C. Guan, W. Huang, *npj Flex. Electron.* 4 (2020) 31, <https://doi.org/10.1038/s41528-020-00093-6>.
- [45] S. Zheng, Z.-S. Wu, S. Wang, H. Xiao, F. Zhou, C. Sun, X. Bao, H.-M. Cheng, *Energy Storage Mater.* 6 (2017) 70–97.
- [46] X. Shi, S. Pei, F. Zhou, W. Ren, H.-M. Cheng, Z.-S. Wu, X. Bao, *Energy Environ. Sci.* 12 (2019) 1534–1541.
- [47] S. Bai, Y. Tang, Y. Wu, J. Liu, H. Liu, W. Yuan, L. Lu, W. Mai, H. Li, Y. Xie, *ACS Appl. Mater. Interfaces* 12 (2020) 45541–45548.
- [48] S. Zheng, W. Lei, J. Qin, Z.-S. Wu, F. Zhou, S. Wang, X. Shi, C. Sun, Y. Chen, X. Bao, *Energy Storage Mater.* 10 (2018) 24–31.
- [49] J. Qin, S. Wang, F. Zhou, P. Das, S. Zheng, C. Sun, X. Bao, Z.-S. Wu, *Energy Storage Mater.* 18 (2019) 397–404.
- [50] S. Wang, Z.-S. Wu, F. Zhou, X. Shi, S. Zheng, J. Qin, H. Xiao, C. Sun, X. Bao, *npj 2D Mater. Appl.* 2 (2018) 7, <https://doi.org/10.1038/s41699-018-0052-8>.
- [51] F. Wan, J. Zhu, S. Huang, Z. Niu, *Batteries Supercaps* 3 (2020) 323–330.
- [52] S. Li, X. Wang, *J. Power Sources* 282 (2015) 394–400.
- [53] Y. Zhu, S. Zheng, P. Lu, J. Ma, P. Das, F. Su, H.-M. Cheng, Z.-S. Wu, *Nat. Sci. Rev.* 9 (2022) nwac024.
- [54] F. Zhou, H. Huang, C. Xiao, S. Zheng, X. Shi, J. Qin, Q. Fu, X. Bao, X. Feng, K. Müllen, Z.-S. Wu, *J. Am. Chem. Soc.* 140 (2018) 8198–8205.
- [55] X. Li, W. Cai, K.S. Teh, M. Qi, X. Zang, X. Ding, Y. Cui, Y. Xie, Y. Wu, H. Ma, Z. Zhou, Q.A. Huang, J. Ye, L. Lin, *ACS Appl. Mater. Interfaces* 10 (2018) 26357–26364.
- [56] Z. Xiong, P. Guo, S. Yuan, S. Sun, C. Wang, Y. Gao, *Energy Fuels* 35 (2021) 16903–16914.
- [57] Y. Shao, M.F. El-Kady, J. Sun, Y. Li, Q. Zhang, M. Zhu, H. Wang, B. Dunn, R.B. Kaner, *Chem. Rev.* 118 (2018) 9233–9280.
- [58] L. Li, J. Zhang, Z. Peng, Y. Li, C. Gao, Y. Ji, R. Ye, N.D. Kim, Q. Zhong, Y. Yang, H. Fei, G. Ruan, J.M. Tour, *Adv. Mater.* 28 (2016) 838–845.
- [59] L. Zhang, P. Zhu, F. Zhou, W. Zeng, H. Su, G. Li, J. Gao, R. Sun, C.P. Wong, *ACS Nano* 10 (2016) 1273–1282.
- [60] J.-X. Feng, S.-H. Ye, A.-L. Wang, X.-F. Lu, Y.-X. Tong, G.-R. Li, *Adv. Funct. Mater.* 24 (2014) 7093–7101.
- [61] M. Naguib, M. Kurtoglu, V. Presser, J. Lu, J. Niu, M. Heon, L. Hultman, Y. Gogotsi, M.W. Barsoum, *Adv. Mater.* 23 (2011) 4248–4253.
- [62] M.R. Lukatskaya, O. Mashtalir, C.E. Ren, Y. Dall’Agnese, P. Rozier, P.L. Taberna, M. Naguib, P. Simon, M.W. Barsoum, Y. Gogotsi, *Science* 341 (2013) 1502–1505.
- [63] M. Ghidui, M.R. Lukatskaya, M.Q. Zhao, Y. Gogotsi, M.W. Barsoum, *Nature* 516 (2014) 78–81.
- [64] B. Anasori, M.R. Lukatskaya, Y. Gogotsi, *Nat. Rev. Mater.* 2 (2017) 16098.
- [65] N. Li, J. Peng, W.-J. Ong, T. Ma, Arramel, P. Zhang, J. Jiang, X. Yuan, C. Zhang, *Matter* 4 (2021) 377–407.
- [66] Y. Zhu, S. Wang, J. Ma, P. Das, S. Zheng, Z.-S. Wu, *Energy Storage Mater.* 51 (2022) 500–526.
- [67] C. Couly, M. Alhabeab, K.L. Van Aken, N. Kurra, L. Gomes, A.M. Navarro-Suárez, B. Anasori, H.N. Alshareef, Y. Gogotsi, *Adv. Electron. Mater.* 4 (2018) 1700339.
- [68] Y. Xie, H. Zhang, H. Huang, Z. Wang, Z. Xu, H. Zhao, Y. Wang, N. Chen, W. Yang, *Nano Energy* 74 (2020).
- [69] F. Zhao, W. Liu, T. Qiu, W.B. Gong, W. Ma, Q. Li, F. Li, F. Geng, *ACS Nano* 14 (2020) 603–610.
- [70] X. Li, Y. Ma, P. Shen, C. Zhang, M. Cao, S. Xiao, J. Yan, S. Luo, Y. Gao, *Adv. Mater. Technol.* 5 (2020) 2000272.
- [71] M. Tahir, L. He, W. Yang, X. Hong, W.A. Haider, H. Tang, Z. Zhu, K.A. Owusu, L. Mai, *J. Energy Chem.* 49 (2020) 224–232.
- [72] K. Shen, J. Ding, S. Yang, *Adv. Energy Mater.* 8 (2018) 1800408.
- [73] Q. Zhang, J. Zhang, Z. Zhou, L. Wei, Y. Yao, *J. Mater. Chem. A* 6 (2018) 20145–20151.
- [74] J. Yin, W. Zhang, N.A. Alhebshi, N. Salah, H.N. Alshareef, *Adv. Energy Mater.* 11 (2021) 2100201.
- [75] G. Sun, H. Yang, G. Zhang, J. Gao, X. Jin, Y. Zhao, L. Jiang, L. Qu, *Energy Environ. Sci.* 11 (2018) 3367–3374.
- [76] N. Wang, T. Xin, Y. Zhao, Q. Li, M. Hu, J. Liu, *ACS Sustain. Chem. Eng.* 7 (2019) 14195–14202.
- [77] P. Zhang, Y. Li, G. Wang, F. Wang, S. Yang, F. Zhu, X. Zhuang, O.G. Schmidt, X. Feng, *Adv. Mater.* 31 (2019) e1806005.
- [78] Z. Huang, A. Chen, F. Mo, G. Liang, X. Li, Q. Yang, Y. Guo, Z. Chen, Q. Li, B. Dong, C. Shi, *Adv. Energy Mater.* 10 (2020) 2001024.
- [79] J. Zeng, L. Dong, L. Sun, W. Wang, Y. Zhou, L. Wei, X. Guo, *Nanomicro Lett.* 13 (2021) 19, <https://doi.org/10.1007/s40820-020-00546-7>.
- [80] Z. Cao, J. Fu, M. Wu, T. Hua, H. Hu, *Energy Storage Mater.* 40 (2021) 10–21.
- [81] Y. Gu, T. Yu, P. Xue, Q. Zhang, S. Ma, X. Xu, *ChemElectroChem* 8 (2021) 4498–4508.
- [82] L. W. Liu, W. Liu, K. Jiang, D. Chen, F. Qu, G. Shen, *Nanomicro Lett.* 13 (2021) 100, <https://doi.org/10.1007/s40820-021-00634-2>.
- [83] X. Li, Y. Ma, Y. Yue, G. Li, C. Zhang, M. Cao, Y. Xiong, J. Zou, Y. Zhou, Y. Gao, *Chem. Eng. J.* 428 (2022).
- [84] Y. Shao, J.H. Fu, Z. Cao, K. Song, R. Sun, Y. Wan, A. Shamim, L. Cavallo, Y. Han, R. B. Kaner, V.C. Tung, *ACS Nano* 14 (2020) 7308–7318.
- [85] S. Zheng, J. Ma, Z.-S. Wu, F. Zhou, Y.-B. He, F. Kang, H.-M. Cheng, X. Bao, *Energy Environ. Sci.* 11 (2018) 2001–2009.
- [86] P. Zhang, L. Wang, F. Wang, D. Tan, G. Wang, S. Yang, M. Yu, J. Zhang, X. Feng, *Batteries Supercaps* 2 (2019) 918–923.
- [87] S. Zheng, S. Wang, Y. Dong, F. Zhou, J. Qin, X. Wang, F. Su, C. Sun, Z.-S. Wu, H.-M. Cheng, X. Bao, *Adv. Sci.* 6 (2019) 1902147.
- [88] S. Zheng, J. Ma, K. Fang, S. Li, J. Qin, Y. Li, J. Wang, L. Zhang, F. Zhou, F. Liu, K. Wang, Z.-S. Wu, *Adv. Energy Mater.* 11 (2021) 2003835.
- [89] Y. Liu, S. Zheng, J. Ma, Y. Zhu, J. Wang, X. Feng, Z.-S. Wu, *J. Energy Chem.* 63 (2021) 514–520.
- [90] J. Yun, Y. Lim, H. Lee, G. Lee, H. Park, S.Y. Hong, S.W. Jin, Y.H. Lee, S.-S. Lee, J.S. Ha, *Adv. Funct. Mater.* 27 (2017) 1700135.
- [91] Y. Shao, J. Li, Y. Li, H. Wang, Q. Zhang, R.B. Kaner, *Mater. Horiz.* 4 (2017) 1145–1150.
- [92] Z.-S. Wu, Y. Zheng, S. Zheng, S. Wang, C. Sun, K. Parvez, T. Ikeda, X. Bao, K. Müllen, X. Feng, *Adv. Mater.* 29 (2017) 1602960.
- [93] Y.-Y. Peng, B. Akuzum, N. Kurra, M.-Q. Zhao, M. Alhabeab, B. Anasori, E.C. Kumbur, H.N. Alshareef, M.-D. Ger, Y. Gogotsi, *Energy Environ. Sci.* 9 (2016) 2847–2854.
- [94] X. Lv, Y. Zhang, X. Li, Z. Fan, G. Liu, W. Zhang, J. Zhou, E. Xie, Z. Zhang, *J. Energy Chem.* 72 (2022) 352–360.
- [95] C. Zhong, Y. Deng, W. Hu, J. Qiao, L. Zhang, J. Zhang, *Chem. Soc. Rev.* 44 (2015) 7484–7539.
- [96] K.-H. Lee, D.B. Ahn, J.-H. Kim, J.-W. Lee, S.-Y. Lee, *Matter* 2 (2020) 345–359.
- [97] P.-Y. Hung, H. Zhang, H. Lin, Q. Guo, K.-T. Lau, B. Jia, *J. Energy Chem.* 68 (2022) 580–602.
- [98] X. Zang, C. Shen, M. Sanghadasa, L. Lin, *ChemElectroChem* 6 (2018) 976–988.
- [99] V.L. Martins, R.M. Torresi, *Curr. Opin. Electrochem.* 21 (2020) 62–68.
- [100] M. Sajjad, M.I. Khan, F. Cheng, W. Lu, *J. Energy Storage* 40 (2021).
- [101] K. Nasrin, S. Gokulnath, M. Karnan, K. Subramani, M. Sathish, *Energy Fuels* 35 (2021) 6465–6482.
- [102] L. Miao, Z. Song, D. Zhu, L. Li, L. Gan, M. Liu, *Energy Fuels* 35 (2021) 8443–8455.
- [103] A. Ray, B. Saruhan, *Materials* 14 (2021) 2942.
- [104] Z. Gao, H. Sun, L. Fu, F. Ye, Y. Zhang, W. Luo, Y. Huang, *Adv. Mater.* 30 (2018) e1705702.
- [105] Z.-S. Wu, S. Yang, L. Zhang, J.B. Wagner, X. Feng, K. Müllen, *Energy Storage Mater.* 1 (2015) 119–126.

- [106] T. Guillemin, C. Douard, K. Robert, B. Asbani, C. Lethien, T. Brousse, J. Le Bideau, *Energy Storage Mater.* 50 (2022) 606–617.
- [107] M.M. Amaral, R. Venâncio, A.C. Peterlevitz, H. Zanin, *J. Energy Chem.* 67 (2022) 697–717.
- [108] L. Suo, O. Borodin, T. Gao, M. Olguin, J. Ho, X. Fan, C. Luo, C. Wang, K. Xu, *Science* 350 (2015) 938–943.
- [109] R.S. Kuhnle, D. Reber, A. Remhof, R. Figi, D. Bleiner, C. Battaglia, *Chem. Commun.* 52 (2016) 10435–10438.
- [110] P. Lannelongue, R. Bouchal, E. Mourad, C. Bodin, M. Olarte, S.I. Vot, F. Favier, O. Fontaine, *J. Electrochem. Soc.* 165 (2018) A657–A663, <https://doi.org/10.1149/2.0951803jes>.
- [111] C. Zhang, J. Holoubek, X. Wu, A. Daniyar, L. Zhu, C. Chen, D.P. Leonard, I.A. Rodriguez-Perez, J.X. Jiang, C. Fang, X. Ji, *Chem. Commun.* 54 (2018) 14097–14099.
- [112] X. Li, H. Li, X. Fan, X. Shi, J. Liang, *Adv. Energy Mater.* 10 (2020) 1903794.
- [113] Y. Zhu, S. Zheng, J. Qin, J. Ma, P. Das, F. Zhou, Z.-S. Wu, *Fund. Res.* (2022), <https://doi.org/10.1016/j.fmre.2022.03.021>.
- [114] Q. Dou, S. Lei, D.-W. Wang, Q. Zhang, D. Xiao, H. Guo, A. Wang, H. Yang, Y. Li, S. Shi, X. Yan, *Energy Environ. Sci.* 11 (2018) 3212–3219.
- [115] X. Jin, L. Song, C. Dai, Y. Xiao, Y. Han, X. Zhang, X. Li, C. Bai, J. Zhang, Y. Zhao, Z. Zhang, L. Jiang, L. Qu, *Adv. Energy Mater.* 11 (2021) 2101523.
- [116] M. Chen, X. Shi, X. Wang, H. Liu, S. Wang, C. Meng, Y. Liu, L. Zhang, Y. Zhu, Z.-S. Wu, *J. Energy Chem.* 72 (2022) 195–202.
- [117] H. Xiao, Z.-S. Wu, L. Chen, F. Zhou, S. Zheng, W. Ren, H.-M. Cheng, X. Bao, *ACS Nano* 11 (2017) 7284–7292.
- [118] P. Zhang, F. Wang, S. Yang, G. Wang, M. Yu, X. Feng, *Energy Storage Mater.* 28 (2020) 160–187.
- [119] K. Keum, J.W. Kim, S.Y. Hong, J.G. Son, S.S. Lee, J.S. Ha, *Adv. Mater.* 32 (2020) e2002180.
- [120] R. Jia, G. Shen, F. Qu, D. Chen, *Energy Storage Mater.* 27 (2020) 169–186.
- [121] H. Hu, K. Zhang, S. Li, S. Ji, C. Ye, *J. Mater. Chem. A* 2 (2014) 20916–20922.
- [122] Z. Liu, Z.-S. Wu, S. Yang, R. Dong, X. Feng, K. Müllen, *Adv. Mater.* 28 (2016) 2217–2222.
- [123] Y. Chen, X. Li, Z. Bi, G. Li, X. He, X. Gao, *Chem. Eng. J.* 353 (2018) 499–506.
- [124] K. Guo, Y. Wan, N. Yu, L. Hu, T. Zhai, H. Li, *Energy Storage Mater.* 11 (2018) 144–151.
- [125] H. Liu, Y. Xie, J. Liu, K.-S. Moon, L. Lu, Z. Lin, W. Yuan, C. Shen, X. Zang, L. Lin, Y. Tang, C.-P. Wong, *Chem. Eng. J.* 393 (2020).
- [126] S. Zheng, X. Tang, Z.-S. Wu, Y.Z. Tan, S. Wang, C. Sun, H.-M. Cheng, X. Bao, *ACS Nano* 11 (2017) 2171–2179.
- [127] X. Shi, L. Tian, S. Wang, P. Wen, M. Su, H. Xiao, P. Das, F. Zhou, Z. Liu, C. Sun, Z.-S. Wu, X. Bao, *J. Energy Chem.* 52 (2021) 284–290.
- [128] X. Pu, M. Liu, L. Li, S. Han, X. Li, C. Jiang, C. Du, J. Luo, W. Hu, Z.L. Wang, *Adv. Energy Mater.* 6 (2016) 1601254.
- [129] Z. Li, D. Lou, K. Chen, W. Jiang, G.S. Han, *Small* 14 (2018) e1702829.
- [130] G. Shao, R. Yu, N. Chen, M. Ye, X.Y. Liu, *Small Methods* 5 (2021) e2000853.
- [131] G. Lee, D. Kim, D. Kim, S. Oh, J. Yun, J. Kim, S.-S. Lee, J.S. Ha, *Energy Environ. Sci.* 8 (2015) 1764–1774.
- [132] G. Lee, J.W. Kim, H. Park, J.Y. Lee, H. Lee, C. Song, S.W. Jin, K. Keum, C.H. Lee, J. S. Ha, *ACS Nano* 13 (2019) 855–866.
- [133] F. Tehrani, M. Beltrán-Gastélum, K. Sheth, A. Karajic, L. Yin, R. Kumar, F. Soto, J. Kim, J. Wang, S. Barton, M. Mueller, *J. Wang, Adv. Mater. Technol.* 4 (2019) 1900162.
- [134] H.J. Yang, J.-W. Lee, S.H. Seo, B. Jeong, B. Lee, W.J. Do, J.H. Kim, J.Y. Cho, A. Jo, H. J. Jeong, S.Y. Jeong, G.-H. Kim, G.-W. Lee, Y.-E. Shin, H. Ko, J.T. Han, J.H. Park, *Nano Energy* 86 (2021).
- [135] L. Li, Z. Lou, W. Han, D. Chen, K. Jiang, G. Shen, *Adv. Mater. Technol.* 2 (2017) 1600282.
- [136] H. Xiao, Z.-S. Wu, F. Zhou, S. Zheng, D. Sui, Y. Chen, X. Bao, *Energy Storage Mater.* 13 (2018) 233–240.
- [137] D. Qi, Z. Liu, Y. Liu, W.R. Leow, B. Zhu, H. Yang, J. Yu, W. Wang, H. Wang, S. Yin, X. Chen, *Adv. Mater.* 27 (2015) 5559–5566.
- [138] S. Jiang, X. Zhou, H. Xiao, W. Chen, X. Xu, Z. Liu, *Chem. Eng. J.* 405 (2021).
- [139] J. Pu, X. Wang, R. Xu, K. Komvopoulos, *ACS Nano* 10 (2016) 9306–9315.
- [140] Y. Lim, J. Yoon, J. Yun, D. Kim, S.Y. Hong, S.J. Lee, G. Zi, J.S. Ha, *ACS Nano* 8 (2014) 11639–11650.
- [141] D. Kim, G. Shin, Y.J. Kang, W. Kim, J.S. Ha, *ACS Nano* 7 (2013) 7975–7982.
- [142] S. Park, H. Lee, Y.-J. Kim, P.S. Lee, *NPG Asia Mater.* 10 (2018) 959–969.
- [143] H.U. Lee, C. Park, J.-H. Jin, S.W. Kim, *J. Power Sources* 453 (2020).
- [144] H. Kim, J. Yoon, G. Lee, S.H. Paik, G. Choi, D. Kim, B.M. Kim, G. Zi, J.S. Ha, *ACS Appl. Mater. Interfaces* 8 (2016) 16016–16025.
- [145] R.K. Pal, S.C. Kundu, V.K. Yadavalli, *ACS Appl. Mater. Interfaces* 10 (2018) 9620–9628.
- [146] P. Das, X. Shi, Q. Fu, Z.-S. Wu, *Adv. Funct. Mater.* 30 (2019) 1908758.
- [147] H. Parsimehr, A. Ehsani, *Chem. Record* 22 (2022) e202200075.
- [148] Y. Yang, D. Yu, H. Wang, L. Guo, *Adv. Mater.* 29 (2017) 1604491.
- [149] Y. Yue, N. Liu, Y. Ma, S. Wang, W. Liu, C. Luo, H. Zhang, F. Cheng, J. Rao, X. Hu, J. Su, Y. Gao, *ACS Nano* 12 (2018) 4224–4232.
- [150] Y. Shi, Y. Wang, Y. Gu, L. Zheng, S. Ma, X. Xu, *Chem. Eng. J.* 392 (2020).
- [151] X. Li, Y. Ma, P. Shen, C. Zhang, J. Yan, Y. Xia, S. Luo, Y. Gao, *ChemElectroChem* 7 (2020) 821–829.
- [152] Y. Wang, Y. Shi, Y. Gu, P. Xue, X. Xu, *Materials* 14 (2021) 1852.
- [153] S. Qin, Q. Zhang, X. Yang, M. Liu, Q. Sun, Z.L. Wang, *Adv. Energy Mater.* 8 (2018) 1800069.
- [154] P. Zhang, F. Zhu, F. Wang, J. Wang, R. Dong, X. Zhuang, O.G. Schmidt, X. Feng, *Adv. Mater.* 29 (2017) 1604491.
- [155] X. Wu, Q. Wang, W. Zhang, Y. Wang, W. Chen, *J. Mater. Sci.* 51 (2016) 7731–7741.
- [156] Z. Liu, H.I. Wang, A. Narita, Q. Chen, Z. Mics, D. Turchinovich, M. Klaui, M. Bonn, K. Müllen, *J. Am. Chem. Soc.* 139 (2017) 9443–9446.
- [157] P. Zhang, J. Wang, W. Sheng, F. Wang, J. Zhang, F. Zhu, X. Zhuang, R. Jordan, O. G. Schmidt, *X. Feng, Energy Environ. Sci.* 11 (2018) 1717–1722.
- [158] H. Zhang, S. Ma, Q. Zhang, M. Cao, Y. Wang, Y. Gu, X. Xu, *ACS Appl. Mater. Interfaces* 12 (2020) 41819–41831.
- [159] X. Tong, Z. Tian, J. Sun, V. Tung, R.B. Kaner, Y. Shao, *Mater. Today* 44 (2021) 78–104.
- [160] X. Wan, C. Xu, *Sci. China Chem.* 60 (2016) 1–2.
- [161] W. Wu, M. Wang, J. Ma, Y. Cao, Y. Deng, *Adv. Electron. Mater.* 4 (2018) 1800185.
- [162] A.A. Argun, P.-H. Aubert, B.C. Thompson, I. Schwendeman, C.L. Gaupp, J. Hwang, N.J. Pinto, D.B. Tanner, A.G. MacDiarmid, J.R. Reynolds, *Chem. Mater.* 16 (2004) 4401–4412.
- [163] J.F. Gohy, Y. Zhao, *Chem. Soc. Rev.* 42 (2013) 7117–7129.
- [164] Z. Tang, H. Gao, X. Chen, Y. Zhang, A. Li, G. Wang, *Nano Energy* 80 (2021).
- [165] S. Rani, N. Kumar, Y. Sharma, *J. Phys. Energy* 3 (2021).
- [166] H. Yang, W.R. Leow, X. Chen, *Adv. Mater.* 30 (2018) e1704347.
- [167] X. Wang, A.Y. Mehandzhyski, B. Arstad, K.L. Van Aken, T.S. Mathis, A. Gallegos, Z. Tian, D. Ren, E. Sheridan, B.A. Grimes, D.E. Jiang, J. Wu, Y. Gogotsi, D. Chen, *Am. Chem. Soc.* 139 (2017) 18681–18687, <https://doi.org/10.1021/jacs.7b10693>.
- [168] A. Patra, J.R. Jose, S. Sahoo, B. Chakraborty, C.S. Rout, *J. Mater. Chem. A* 9 (2021) 25852–25891.
- [169] H. Li, S. Guo, H. Zhou, *J. Energy Chem.* 59 (2021) 191–211.
- [170] X. Su, J. Ye, Y. Zhu, *J. Energy Chem.* 54 (2021) 242–253.
- [171] S. Sollami Delekt, A.D. Smith, J. Li, M. Ostling, *Nanoscale* 9 (2017) 6998–7005.
- [172] J. Li, Q. Shi, Y. Shao, C. Hou, Y. Li, Q. Zhang, H. Wang, *Energy Storage Mater.* 16 (2019) 212–219.
- [173] V. Raman, D. Rhee, A.R. Selvaraj, J. Kim, K. Prabakar, J. Kang, H.K. Kim, *Sci. Technol. Adv. Mater.* 22 (2021) 875–884.
- [174] X. Guan, L. Pan, Z. Fan, *Membranes* 111 (2021) 788.
- [175] Q. Jiang, N. Kurra, K. Maleski, Y. Lei, H. Liang, Y. Zhang, Y. Gogotsi, H.N. Alshareef, *Adv. Energy Mater.* (2019) 1901061.
- [176] X. Feng, S. Wang, P. Das, X. Shi, S. Zheng, F. Zhou, J. Ning, D. Wang, J. Zhang, Y. Hao, Z.-S. Wu, *J. Energy Chem.* 69 (2022) 1–8.
- [177] T. Yu, Y. Wang, K. Jiang, G. Zhai, C. Ke, J. Zhang, J. Li, D. Tranca, E. Kymakis, X. Zhuang, *Chemistry* 27 (2021) 6340–6347.
- [178] I. Khakpour, A.R. Baboukani, S. Forouzanfar, A. Allagui, C. Wang, *J. Power Sources* 516 (2021).
- [179] D. Zhao, W. Chang, C. Lu, C. Yang, K. Jiang, X. Chang, H. Lin, F. Zhang, S. Han, Z. Hou, X. Zhuang, *Small* 15 (2019) e1901494.
- [180] C. Yang, K.S. Schellhammer, F. Ortmann, S. Sun, R. Dong, M. Karakus, Z. Mics, M. Löffler, F. Zhang, X. Zhuang, E. Canovas, G. Cuniberti, M. Bonn, X. Feng, *Angew. Chem. Int. Ed.* 56 (2017) 3920–3924.
- [181] N. Kurra, M.K. Hota, H.N. Alshareef, *Nano Energy* 13 (2015) 500–508.
- [182] W. Zhao, M. Jiang, W. Wang, S. Liu, W. Huang, Q. Zhao, *Adv. Funct. Mater.* 31 (2020) 2009136.
- [183] H. Zhang, *ACS Nano* 9 (2015) 9451–9469.
- [184] A.K. Geim, *Science* 324 (2009) 1530–1534.
- [185] S. Manzeli, D. Ovchinnikov, D. Pasquier, O.V. Yazyev, A. Kis, *Nat. Rev. Mater.* 2 (2017) 17033.
- [186] X. Feng, X. Shi, J. Ning, D. Wang, J. Zhang, Y. Hao, Z.-S. Wu, *eScience* 1 (2021) 124–140.
- [187] H. Tang, Y. Tian, Z. Wu, Y. Zeng, Y. Wang, Y. Hou, Z. Ye, J. Lu, *Energy Environ. Mater.* 5 (2022) 1060–1083.
- [188] C. Xu, C. Pan, Y. Liu, Z.L. Wang, *Nano Energy* 1 (2012) 259–272.
- [189] M. Gao, P. Wang, L. Jiang, B. Wang, Y. Yao, S. Liu, D. Chu, W. Cheng, Y. Lu, *Energy Environ. Sci.* 14 (2021) 2114–2157.
- [190] J. Qiu, Y. Shen, B. Li, Y. Zheng, Y. Xia, Y. Chen, W. Huang, *Solar RRL* 3 (2019) 1900320.
- [191] J. Luo, Z.L. Wang, *Energy Storage Mater.* 3 (2019) 617–628.
- [192] H. Nazemi, A. Joseph, J. Park, A. Emadi, *Sensors* 19 (2019) 1285.
- [193] J. Wu, Y. Zheng, X. Li, *Sensors* 21 (2021) 7129.
- [194] Z. Lou, L. Li, G.S. Wang, *Small* 13 (2017) 1701791.
- [195] P.C.Y. Chow, T. Someya, *Adv. Mater.* 32 (2020) e1902045.
- [196] J. Zhao, J. Zha, Z. Zeng, C. Tan, *J. Mater. Chem. A* 9 (2021) 18887–18905.
- [197] P. Jiao, *Nano Energy* 88 (2021).
- [198] K. Zhang, Y. Wang, Y. Yang, *Adv. Funct. Mater.* 29 (2018) 1806435.
- [199] Y. He, K. Chen, M.K.H. Leung, Y. Zhang, L. Li, G. Li, J. Xuan, J. Li, *Chem. Eng. J.* 428 (2022).
- [200] M. Qiu, P. Sun, G. Cui, Y. Tong, W. Mai, *ACS Nano* 13 (2019) 8246–8255.
- [201] S.W. Lee, S. Bae, D. Kim, H.S. Lee, *Adv. Mater.* 32 (2020) e2002202.
- [202] Q. Jiang, C. Wu, Z. Wang, A.C. Wang, J.-H. He, Z.L. Wang, H.N. Alshareef, *Nano Energy* 45 (2018) 266–272.
- [203] L.V. Thekkekkara, B. Jia, Y. Zhang, L. Qiu, D. Li, M. Gu, *Appl. Phys. Lett.* 107 (2015).
- [204] W. Tian, Y. Wang, L. Chen, L. Li, *Small* 13 (2017) 1701848.
- [205] Y. Lu, K. Jiang, D. Chen, G. Shen, *Nano Energy* 58 (2019) 624–632.
- [206] J. Qin, J. Gao, X. Shi, J. Chang, Y. Dong, S. Zheng, X. Wang, L. Feng, Z.-S. Wu, *Adv. Funct. Mater.* 30 (2020) 1909756.
- [207] D. Kim, D. Kim, H. Lee, Y.R. Jeong, S.J. Lee, G. Yang, H. Kim, G. Lee, S. Jeon, G. Zi, J. Kim, J.S. Ha, *Adv. Mater.* 28 (2016) 748–756.

- [208] L. Li, C. Fu, Z. Lou, S. Chen, W. Han, K. Jiang, D. Chen, G. Shen, *Nano Energy* 41 (2017) 261–268.
- [209] J. Ye, H. Tan, S. Wu, K. Ni, F. Pan, J. Liu, Z. Tao, Y. Qu, H. Ji, P. Simon, Y. Zhu, *Adv. Mater.* 31 (2018) e1801384.
- [210] J. Yun, Y. Lim, G.N. Jang, D. Kim, S.-J. Lee, H. Park, S.Y. Hong, G. Lee, G. Zi, J.S. Ha, *Nano Energy* 19 (2016) 401–414.
- [211] L. Li, Z. Lou, W. Han, G. Shen, *Nanoscale* 8 (2016) 14986–14991.
- [212] Y. Song, H. Chen, X. Chen, H. Wu, H. Guo, X. Cheng, B. Meng, H. Zhang, *Nano Energy* 53 (2018) 189–197.
- [213] C. Chen, J. Cao, X. Wang, Q. Lu, M. Han, Q. Wang, H. Dai, Z. Niu, J. Chen, S. Xie, *Nano Energy* 42 (2017) 187–194.
- [214] R. Guo, J. Chen, B. Yang, L. Liu, L. Su, B. Shen, X. Yan, *Adv. Funct. Mater.* 27 (2017) 1702394.
- [215] D. Kim, J. Yun, G. Lee, J.S. Ha, *Nanoscale* 6 (2014) 12034–12041.
- [216] Y.S. Moon, D. Kim, G. Lee, S.Y. Hong, K.K. Kim, S.M. Park, J.S. Ha, *Carbon* 81 (2015) 29–37.
- [217] S. Gu, Z. Lou, L. Li, Z. Chen, X. Ma, G. Shen, *Nano Res.* 9 (2016) 424–434.
- [218] J. Xu, G. Shen, *Nano Energy* 13 (2015) 131–139.
- [219] X.-J. Huang, Y.-K. Choi, *Sens. Actuators B Chem.* 122 (2007) 659–671.
- [220] S. Li, Y. Zhang, Y. Wang, K. Xia, Z. Yin, H. Wang, M. Zhang, X. Liang, H. Lu, M. Zhu, H. Wang, X. Shen, Y. Zhang, *InfoMat* 2 (2019) 184–211.
- [221] J. Yun, C. Song, H. Lee, H. Park, Y.R. Jeong, J.W. Kim, S.W. Jin, S.Y. Oh, L. Sun, G. Zi, J.S. Ha, *Nano Energy* 49 (2018) 644–654.
- [222] J. Cai, C. Lv, *Nano Energy* 30 (2016) 790–800.
- [223] Y. Song, H. Wang, X. Cheng, G. Li, X. Chen, H. Chen, L. Miao, X. Zhang, H. Zhang, *Nano Energy* 55 (2019) 29–36.
- [224] C. Zhang, Z. Peng, C. Huang, B. Zhang, C. Xing, H. Chen, H. Cheng, J. Wang, S. Tang, *Nano Energy* 81 (2021).
- [225] X. Shi, J. Chang, J. Qin, H. Liu, X. Zhang, Y. Ma, J. He, X. Chou, L. Feng, Z.-S. Wu, X. Bao, *Nano Energy* 88 (2021).
- [226] J. Ma, S. Zheng, Y. Cao, Y. Zhu, P. Das, H. Wang, Y. Liu, J. Wang, L. Chi, S. Liu, Z.-S. Wu, *Adv. Energy Mater.* 11 (2021) 2100746.
- [227] Y. Zhang, Y. Zhu, S. Zheng, L. Zhang, X. Shi, J. He, X. Chou, Z.-S. Wu, *J. Energy Chem.* 63 (2021) 498–513.
- [228] W. Zhang, H. Liu, X. Zhang, X. Li, G. Zhang, P. Cao, *Adv. Funct. Mater.* 31 (2021) 2104909.
- [229] F. Li, M. Huang, J. Wang, J. Qu, Y. Li, L. Liu, V.K. Bandari, Y. Hong, B. Sun, M. Zhu, F. Zhu, Y.X. Zhang, O.G. Schmidt, *Energy Storage Mater.* 27 (2020) 17–24.
- [230] X. Zhou, P.S. Lee, *EcoMat* 3 (2021) e12098.
- [231] B. Chen, W. Tang, Z.L. Wang, *Mater. Today* 50 (2021) 224–238.
- [232] V. Egorov, U. Gulzar, Y. Zhang, S. Breen, C. O'Dwyer, *Adv. Mater.* 32 (2020) e2000556.
- [233] Y. Xu, X. Wu, X. Guo, B. Kong, M. Zhang, X. Qian, S. Mi, W. Sun, *Sensors* 17 (2017) 1166.
- [234] H. Liu, H. Zhang, W. Han, H. Lin, R. Li, J. Zhu, W. Huang, *Adv. Mater.* 33 (2021) e2004782.